




# A Filippov Model Describing the Effect of Social Distancing in Controlling Infectious Diseases

Aili Wang<sup>1</sup> · Yinjiao Gong<sup>2</sup> · Duo Bai<sup>1</sup> · Weike Zhou<sup>3</sup> · Stacey R. Smith<sup>4</sup> 

Received: 31 January 2025 / Accepted: 30 August 2025

© The Author(s), under exclusive licence to the Society for Mathematical Biology 2025

## Abstract

Social distancing is now a familiar strategy for managing disease outbreaks, but it is important to understand the interaction between disease dynamics and social behaviour. We distinguished the fully susceptibles from the social-distancing susceptibles and proposed a Filippov epidemic model to study the effect of social distancing on the spread and control of infectious diseases. The threshold policy is defined as follows: once the number of infected individuals exceeds the threshold value, social-distancing susceptibles take more stringent social-distancing practices, resulting in a decreasing infection rate. The target model exhibits novel dynamics: in addition to the coexistence of two attractors, it also demonstrates the coexistence of three attractors. In particular, bistability of the regular endemic equilibrium and the disease-free equilibrium occurs for the system; multistability of the regular endemic equilibrium, a pseudo-equilibrium and the disease-free equilibrium also occurs for the system. Discontinuity-induced bifurcations, including boundary-node, focus and saddle-node bifurcations, occur for the proposed model, which reveals that a small change in threshold values would significantly affect the outcome. Our findings indicate that for a proper threshold value, the infections can be ruled out or contained at the previously given level if the initial infection is relatively small.

**Keywords** Filippov model · Social-distancing · Sliding dynamics · Boundary equilibrium bifurcation · Global dynamics

---

✉ Aili Wang  
wangal@xaut.edu.cn

✉ Stacey R. Smith?  
stacey.smith@uottawa.ca

<sup>1</sup> School of Science, Xi'an University of Technology, Xi'an 710054, People's Republic of China

<sup>2</sup> School of Mathematics and Information Science, Baoji University of Arts and Sciences, Baoji 721013, People's Republic of China

<sup>3</sup> School of Mathematics, Northwest University, Xi'an 710127, Shaanxi, People's Republic of China

<sup>4</sup> Department of Mathematics and Faculty of Medicine, The University of Ottawa, Ottawa K1N 6N5, ON, Canada

## 1 Introduction

Since the beginning of the COVID-19 pandemic, it has become clear that non-pharmaceutical interventions, including social distancing, can be used to control epidemics. Social distancing, a practice of keeping physical distance between individuals during social interactions, plays a vital role in the battle against infectious diseases (Stockmaier et al. 2021). It acts as a potent barrier to the direct dissemination of pathogens, particularly those transmitted via respiratory droplets, exemplified by influenza and COVID-19 (World Health Organization 2021; Yan et al. 2021). Chu et al. found that keeping a distance of at least one metre reduced the risk of transmission of many respiratory illness by 82% (Chu et al. 2020). Since the spread of infectious diseases is a complex process involving multiple routes of transmission, social distancing can help break the chain of transmission by minimizing direct and indirect contacts between infected and susceptible individuals, which, in turn, slows down the spread of the disease. Koo et al. found that the combined intervention of quarantining infected individuals and their family members, workplace distancing and school closures could reduce the estimated median number of infections by 93% (Koo et al. 2020). Although ‘social distancing’ is now an familiar measure to combat infectious diseases, we still have much to learn about its underlying mechanisms and epidemiological consequences.

The precise nature of social distancing is dynamic and heterogeneous, changing in response to the evolving epidemic. Zhang et al. (2023) and Chen et al. (2024) showed that during the COVID-19 outbreak in Shanghai, population mobility progressively declined through successive phases — from targeted interventions to a citywide lockdown — reflecting a substantial intensification of social-distancing measures; similarly, during the acute phase of the global pandemic, stringent non-pharmaceutical interventions, including social distancing and travel restrictions, led to a marked reduction in both influenza transmission and human mobility worldwide. Zheng et al. (2023) further identified that the spatiotemporal spread of the Omicron variant was significantly influenced by localized mobility patterns, highlighting the critical role of behavioral adaptations and interventions at the subdistrict level. Li et al. (2024) developed a mathematical model incorporating behavioral imitation, showing that individuals’ willingness to adopt social distancing was closely tied to perceived infection risk. They underscored that social distancing is an adaptive behavior, influenced by perceived risk, public policy and socio-demographic factors, evolving dynamically over the course of an outbreak.

Many studies have been dedicated to understanding how and to what extent social-distancing behaviours affect the transmission of infectious diseases qualitatively and quantitatively. Maharaj and Kleczkowski (2012) studied the costs and benefits of individual-based social distancing using an SIR model and found that social distancing can be effective but may require prolonged measures to prevent disease rebound. Lobinska et al. (2022) analyzed the probability of emergence of vaccine-resistant strains under varying degrees of social distancing and suggested maintaining social distancing until herd immunity was achieved. Gollwitzer et al. (2022) examined the link between self-reported and objective social distancing and found that self-reported distancing measures can predict actual distancing behaviour. Duan et al. (2022) and

Gong et al. (2022) applied an integrated social-cognition model to predict social distancing among older adults during COVID-19. Their findings highlight the importance of health knowledge and motivational self-efficacy. Matrajt and Leung (2020) and Ventura et al. (2022) modelled the effect of social distancing by reducing the contact rates between individuals in compartment models. Their findings underscore that rigorous social distancing can effectively mitigate the spread of an epidemic, but less stringent measures can contain the transmission but potentially elevate the mortality rate. Tang et al. (2022), Di Guilmi et al. (2022) and d'Onofrio and Manfredi (2022) extended the classical SEIR model to study the co-evolution of behavioural changes and COVID-19, incorporating heterogeneity among those who practice social distancing. They found that behavioural changes significantly affected disease-transmission dynamics. Huang et al. (2021) developed a communication-contact two-layer network model to analyze the impact of public social distancing on an infectious disease with asymptomatic infection and found that social distancing can substantially increase the outbreak threshold. Dashtbali and Mirzaie (2021) and Saha et al. (2022) formulated compartmental models to reveal the effect of social distancing and vaccination in controlling COVID-19. Their results showed that a combination of vaccination and social distancing could effectively reduce disease burden. Chen et al. (2023) proposed an epidemic control framework using mobility data to set efficient social-distancing targets. They proposed an efficient social-distancing policy to minimize the aggregated risks of disease and economic loss.

These studies underscore the crucial role of social distancing in mitigating the spread of infectious diseases utilizing various models, including behavioural and social psychological models, epidemiological models, agent-based models and network models. However, most of the existing epidemic models have largely tended to neglect the impact of individual awareness of the presence of diseases. Instead, the structure of interactions between individuals is most commonly assumed to be an average behavioural pattern. In fact, there exists a significant relationship between an individual's risk perception and their willingness to engage in preventive measures including social distancing (Dryhurst et al. 2022). Individuals who possess a comprehensive understanding of a disease's severity are more likely to adhere to preventive measures, while those with limited knowledge or an underestimated perception of the threat may neglect these crucial preventive measures (Brewer et al. 2007; Kristiansen et al. 2007). Epstein et al. (2008) and Mpeshe and Nyerere (2021) developed epidemic models that incorporated distinct groups of susceptibles and infecteds, categorizing them based on their susceptibility to fear. They found that fear can significantly affect the dynamics of epidemics, with even small levels of fear-inspired flight dramatically altering disease spread. Jain et al. (2022) presented an individual-based fear model with variations in individual fear levels, which was updated based on the changing size of the epidemic. Their findings suggested that fear can suppress disease transmission but also lead to multiple epidemic waves. Collinson et al. (2015) and Gevertz et al. (2021) presented an epidemiological model with explicit compartments for susceptible and asymptomatic individuals who socially distance due to variations in individual fear levels. Their findings demonstrated that social distancing can effectively reduce disease transmission but requires timely implementation. Misra et al. (2011) and Samanta et al. (2013) modelled the impact of media on the spread of infectious diseases, con-

sidering variations in infectivity within the susceptible population. They found that enhanced media reporting can effectively reduce infections.

These models take into account the differences in social-distancing measures adopted by different individuals during an outbreak. In practice, individuals who adopt social-distancing measures implement stricter practices once the epidemic becomes more severe. Hence, we introduce a piecewise function to describe the consequences of intensifying social-distancing measures when the epidemic intensifies, leading to the formulation of a Filippov model. Filippov systems have been successfully applied in epidemic control. They investigated the effect of variable structure control on the psychological impact, media effect, quarantine and delay on the containment of infectious diseases (Wang et al. 2022). Xiao et al. 2012, Wang and Xiao 2014 and Zhang et al. 2024 modelled the effect of media-induced social distancing on disease transmission by incorporating piecewise incidence rates into classical models, where control or precautionary measures are activated once the number of infected individuals surpasses a predefined threshold. Xiao et al. 2015, Wang et al. 2020 and Deng et al. 2021 mimicked the behavioural response induced by media by incorporating piecewise incidence rates that modify the transmission rate once media impact is activated, with threshold-based controls triggered by both the number of infections and its rate of change. Cherif et al. (2016) developed an *in silico* model of pathogen avoidance, where entry into the behavioural class depends on a behavioural cue and psychological threshold. Its mean-field approximation leads to a Filippov system capturing the resulting non-smooth dynamics.

Many of these models have addressed how social distancing affects the spread of epidemic diseases using Filippov models, where all susceptibles are assumed to adopt an identical level of social-distancing, without distinguishing between different behavioural responses. In particular, they did not differentiate between susceptible individuals who practice social distancing and those who do not, nor did they account for the possibility that susceptibles practicing social distancing may strengthen their distancing behaviour once the epidemic intensifies. We will investigate both aspects.

## 2 Filippov Model

We consider a threshold policy in a dynamical model, which consists of three compartments: fully susceptible ( $S$ ), social-distancing susceptibles ( $S_M$ ) and infected individuals ( $I$ ), where ‘social-distancing susceptibles’ describes those individuals who are media aware and less susceptible to infection due to social-distancing behaviours. We assume that susceptible individuals can be exposed to the virus either directly or after moving into the social-distancing-susceptible compartment. Social-distancing susceptibles have lower probability of transmission compared to the fully susceptibles, since they will take more precautions. Social-distancing susceptibles relax from social-distancing practices and move back into the fully susceptible compartment at a rate of  $\mu$ , so  $1/\mu$  represents the average time that social-distancing susceptibles spend while social distancing. Let  $\Lambda$  represent the natural birth rate,  $\gamma$  represent the recovery rate,  $k$  represent the reinforcement factor,  $\lambda$  represent the progression rate from fully susceptible to social-distancing susceptible and  $d$  represent the natural death

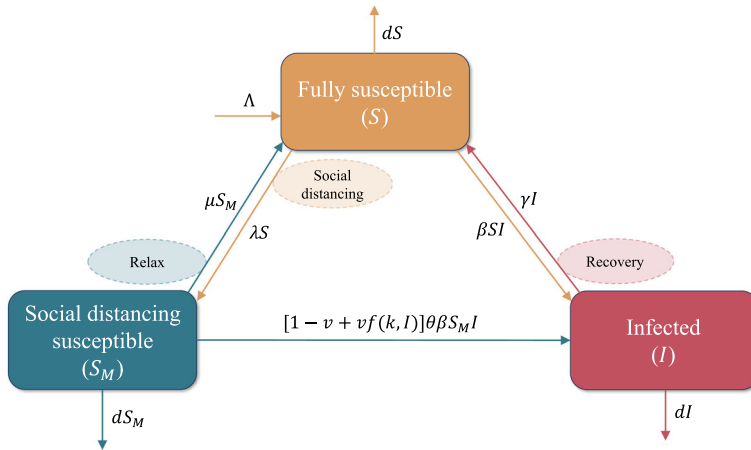


**Fig. 1** A schematic flow diagram of the transmission of disease with social-distancing practices

rate. We assume the transmission rate between infecteds and fully susceptibles (resp., social-distancing susceptibles) is  $\beta$  (resp.,  $\theta\beta$ ) and  $\beta > d + \gamma$ , where  $0 < \theta < 1$  is a constant. When the reported number of infected individuals exceeds a critical level  $I_c$ , social-distancing susceptibles will take more stringent social-distancing practices, which results in a decline in the transmission between  $I$  and  $S_M$ . We thus multiply the transmission rate  $\theta\beta$  by a factor  $f(k, I)$ , which accounts for the decline in the transmission due to more stringent social-distancing practices. Here,  $0 < f(k, I) < 1$ , and the parameter  $k$  reflects the level of social-distancing reinforcement increases and that it also decreases as the number of infected individuals increases; i.e.,  $f(k, I)$  satisfies

$$\frac{\partial f(k, I)}{\partial k} < 0, \quad \frac{\partial f(k, I)}{\partial I} < 0.$$

In disease-control practices, any function that meets the above conditions can be used as  $f(k, I)$ . Our model is illustrated in Fig. 1.

To illustrate our main idea, we assume all infected individuals return to full susceptibility upon recovery. This is reasonable for some infectious diseases, such as schistosomiasis and brucellosis. Colley et al. (2014) and Diaby (2015) demonstrated that people recovering from schistosomiasis typically do not develop complete or sterile immunity, indicating that reinfection remains common in the absence of sustained preventive interventions. Zhang et al. (2024) indicated that recovery from brucellosis does not confer effective or long-lasting immunity; instead, individuals are susceptible to reinfection. Therefore, our Filippov model is described by differential equations with discontinuous right-hand sides as follows:

**Table 1** Definitions of parameters for model (1)

Parameters	Definition
$\Lambda$	Natural birth rate
$\beta$	Transmission rate between infecteds and fully susceptibles
$\gamma$	Recovery rate of infected individuals
$d$	Natural death rate
$\theta$	Relative transmission probability of social distancing susceptibles compared with fully susceptibles
$k$	Reinforcement factor
$\frac{1}{\mu}$	Average time that social-distancing susceptibles spend while social distancing
$\lambda$	Progression rate from fully susceptibles to social distancing susceptibles

$$\begin{aligned}
 \frac{dS}{dt} &= \Lambda - \beta SI - \lambda S + \gamma I + \mu S_M - dS, \\
 \frac{dS_M}{dt} &= \lambda S - [1 - v + v f(k, I)] \theta \beta S_M I - \mu S_M - dS_M, \\
 \frac{dI}{dt} &= \beta SI + [1 - v + v f(k, I)] \theta \beta S_M I - \gamma I - dI,
 \end{aligned} \tag{1}$$

with

$$v = \begin{cases} 0, & \sigma(I) < 0, \\ 1, & \sigma(I) > 0, \end{cases} \tag{2}$$

where  $\sigma(I)$  is a control function that depends on the number of infected individuals. In infectious-disease-control practices, the specific form of the function  $\sigma(I)$  can be derived from the implementation strategy of the control measures. Its form may be linear or nonlinear. To illustrate our idea, we choose the function  $\sigma(I) = I - I_c$ , which suggests that when the number of infected individuals is greater than the threshold value  $I_c$ , social-distancing susceptibles will adopt more stringent precautions, which will lead to a significant drop in their contacts. Model (1) with (2) is a dynamical system controlled by a threshold policy. For convenience, we list the definitions of each parameter in Table 1.

Letting  $N(t) = S(t) + S_M(t) + I(t)$ , we get

$$\frac{dN}{dt} = \Lambda - dN.$$

For simplicity, we can assume  $\Lambda = d$ , and it follows that  $\lim_{t \rightarrow \infty} N(t) = 1$ , so we only need to consider the following simplified system:

$$\begin{aligned}\frac{dS_M}{dt} &= \lambda(1 - I - S_M) - [1 - v + v f(k, I)]\theta\beta S_M I - \mu S_M - dS_M, \\ \frac{dI}{dt} &= (\beta - \gamma - d)I - \beta \left[ 1 - (1 - v + v f(k, I))\theta \right] S_M I - \beta I^2.\end{aligned}\quad (3)$$

It is easy to show that

$$\Omega = \{(S_M, I) \in R_+^2 | 0 < S_M(t) + I(t) \leq 1\}$$

is an attraction region of system (3). The discontinuous switching surface is  $\Sigma = \{(S_M, I) \in \Omega | \sigma(I) = 0\}$ , and it divides space into the following two subregions:

$$G_1 = \{(S_M, I) \in \Omega | \sigma(I) < 0\}, \quad G_2 = \{(S_M, I) \in \Omega | \sigma(I) > 0\}.$$

Thus, social-distancing susceptibles take moderate social-distancing practices and the transmission rate takes the form  $\beta\theta$  in the subregion  $G_1$ ; while in region  $G_2$ , they take more stringent social-distancing practices, and hence the transmission rate switches to  $f(k, I)\beta\theta$ . The system defined on the subregion  $G_i$  ( $i = 1, 2$ ) is called Subsystem  $S_{G_i}$ . Letting  $Z = (S_M, I)^T$ , we have

$$\frac{dZ}{dt} = \begin{cases} F_{G_1}(Z), & Z \in G_1, \\ F_{G_2}(Z), & Z \in G_2, \end{cases}\quad (4)$$

where  $F_{G_i}(Z) = (f_{i1}(Z), f_{i2}(Z))^T$  ( $i = 1, 2$ ) and

$$\begin{aligned}f_{11}(S_M, I) &= \lambda(1 - I) - (\lambda + \mu + d)S_M - \beta\theta S_M I, \\ f_{12}(S_M, I) &= (\beta - \gamma - d)I - \beta(1 - \theta)S_M I - \beta I^2, \\ f_{21}(S_M, I) &= \lambda(1 - I) - (\lambda + \mu + d)S_M - f(k, I)\theta\beta S_M I, \\ f_{22}(S_M, I) &= (\beta - \gamma - d)I - \beta[1 - f(k, I)\theta]S_M I - \beta I^2.\end{aligned}$$

For simplicity, we also call Subsystem  $S_{G_1}$  the free system, and we call Subsystem  $S_{G_2}$  the control system. We next introduce the following technical definitions in order to further examine the dynamics of model (4).

**Definition 1** Let  $Z_*$  be an equilibrium of subsystem  $S_{G_i}$  ( $i = 1, 2$ ). Then  $Z_*$  is called a real (resp., virtual) equilibrium of Filippov system (4) if one of the following conditions are satisfied:

- $F_{G_1}(Z_*) = 0$ ,  $Z_* \in G_1$  (resp  $Z_* \in G_2$ );
- $F_{G_2}(Z_*) = 0$ ,  $Z_* \in G_2$  (resp  $Z_* \in G_1$ ).

Both real equilibria (denoted as  $Z_*^r$ ) and virtual equilibria (denoted as  $Z_*^v$ ) are called regular equilibria.

According to Definition 1, an equilibrium of Subsystem  $S_{G_1}$  (resp.,  $S_{G_2}$ ) is said to be real if it lies in the subregion  $G_1$  (resp.,  $G_2$ ); i.e., if it exists inside its own subsystem. An equilibrium is virtual if it lies outside its own subsystem.

**Definition 2** Let  $Z_*$  satisfy  $\sigma(Z_*) = 0$ . Then  $Z_*$  is called a pseudo-equilibrium of Filippov system (4) if it satisfies  $\xi F_{G_1}(Z_*) + (1 - \xi)F_{G_2}(Z_*) = 0$  with

$$\xi = \frac{F_{G_2}\sigma(Z_*)}{(F_{G_2} - F_{G_1})\sigma(Z_*)},$$

where  $F_{G_i}\sigma(Z_*)$  represents the Lie derivative (Willmore 1960) of  $\sigma$  with respect to the vector field  $F_{G_i}$  at the point  $Z_*$  and  $F_{G_i}\sigma(Z_*) = F_{G_i}(Z_*) \cdot \text{grad}\sigma(Z_*)$ . We call a pseudo-equilibrium  $Z_*$  admissible if  $0 < \xi < 1$ . Alternately, a pseudo-equilibrium  $Z_*$  is called virtual if  $\xi < 0$  or  $\xi > 1$ .

Definition 2 indicates that a pseudo-equilibrium  $Z_*$  is said to be admissible if it lies in the domain of the sliding-mode region; otherwise, it is said to be virtual. Pseudo-equilibria are not equilibria of the ODEs, but are a consequence of the Filippov boundary.

**Definition 3** A point  $Z_*$  is called a tangent point of Filippov system (4) if  $Z_* \in \Sigma$  and  $F_{G_1}\sigma(Z_*) = 0$  or  $F_{G_2}\sigma(Z_*) = 0$ . A smooth vector field  $F_{G_i}$  ( $i = 1, 2$ ) has a fold or quadratic tangency with  $\sigma$  at a point  $Z_*$  provided  $F_{G_i}\sigma(Z_*) = 0$  and  $F_{G_i}^2\sigma(Z_*) \neq 0$ . Moreover, a fold tangency point  $Z_*$  is said to be visible (resp. invisible) if  $F_{G_1}^2\sigma(Z_*) < 0$  (resp.  $F_{G_1}^2\sigma(Z_*) > 0$ ) or  $F_{G_2}^2\sigma(Z_*) > 0$  (resp.  $F_{G_2}^2\sigma(Z_*) < 0$ ).

It follows from Definition 3 that a tangent point of Filippov system (4) refers to an endpoint of the sliding-mode region that lies in the interior of the first quadrant.

**Definition 4** A point  $Z_*$  is called a boundary equilibrium of Filippov system (4) if  $F_{G_1}(Z_*) = 0$ ,  $\sigma(Z_*) = 0$  or  $F_{G_2}(Z_*) = 0$ ,  $\sigma(Z_*) = 0$ . If  $Z_*$  is the boundary equilibrium of Filippov system (4) and  $\det(DF_{G_i}(Z_*)) \neq 0$ ,  $i = 1, 2$ , then a boundary equilibrium bifurcation occurs at the point  $Z_*$ .

We know from Definition 4 that an equilibrium of Filippov system (4) is called a boundary equilibrium if it hits the sliding-mode region exactly on one of the endpoints.

For convenience, we adopt the following particular form for the social-distancing reinforcement factor:  $f(k, I) = \frac{1}{1 + kI}$ . Hence model (3) becomes

$$\begin{aligned} \frac{dS_M}{dt} &= \lambda(1 - I - S_M) - \frac{\theta\beta S_M I}{1 + vkI} - \mu S_M - dS_M, \\ \frac{dI}{dt} &= (\beta - \gamma - d)I - \beta \left(1 - \frac{\theta}{1 + vkI}\right) S_M I - \beta I^2. \end{aligned} \quad (5)$$

### 3 Dynamics of the Two Subsystems $S_{G_i}$ ( $i = 1, 2$ )

We will investigate the dynamics of the two subsystems  $S_{G_i}$  ( $i = 1, 2$ ) in this section, including all the possible equilibria and their stabilities.



### 3.1 Dynamics of the Free System

For Subsystem  $S_{G_1}$ , there always exists a unique disease-free equilibrium  $E_{10} = \left(\frac{\lambda}{\lambda + \mu + d}, 0\right)$ . The basic reproduction number is calculated as

$$\mathcal{R}_0 = \frac{\beta(\theta\lambda + d + \mu)}{(\lambda + \mu + d)(d + \gamma)}$$

by using the next-generation-matrix method. The endemic equilibrium of subsystem  $S_{G_1}$  satisfies

$$\begin{aligned} a_{11}I^2 + a_{12}I + a_{13} &= 0, \\ S_M &= \frac{\beta - \gamma - d - \beta I}{\beta(1 - \theta)}, \end{aligned} \quad (6)$$

where

$$\begin{aligned} a_{11} &= \beta^2\theta, \quad a_{12} = \beta[\theta(\lambda - \beta + d + \gamma) + \mu + d], \\ a_{13} &= (d + \gamma)(\lambda + \mu + d)(1 - \mathcal{R}_0). \end{aligned}$$

Denote  $g_1(I) = a_{11}I^2 + a_{12}I + a_{13}$ . If  $\mathcal{R}_0 > 1$ , it is easy to see that  $a_{11} > 0$  and  $a_{13} < 0$ , so a unique positive root  $I_{12} = \frac{-a_{12} + \sqrt{\Delta_1}}{2a_{11}}$  exists for the first equation of (6), where  $\Delta_1 = a_{12}^2 - 4a_{11}a_{13}$ . Direct calculation yields that

$$g_1\left(\frac{\beta - \gamma - d}{\beta}\right) > 0 \implies 0 < I_{12} < \frac{\beta - \gamma - d}{\beta}.$$

It follows that

$$S_{M_{12}} = \frac{\beta - \gamma - d - \beta I_{12}}{\beta(1 - \theta)} > 0,$$

so a unique positive equilibrium  $E_{12} = (S_{M_{12}}, I_{12})$  exists for Subsystem  $S_{G_1}$  for  $\mathcal{R}_0 > 1$ .

For  $\mathcal{R}_0 < 1$ , we can get  $a_{11} > 0$  and  $a_{13} > 0$ , so the existence of positive solutions of (6) depends on  $a_{12}$  and  $\Delta_1$ . Denote

$$R_{c1} = \frac{\beta\theta(\beta - \gamma - d)}{2\sqrt{a_{11}a_{13}} + a_{12} + \beta\theta(\beta - \gamma - d)}.$$

If  $R_{c1} > 1$ , we have  $a_{12} < 0$  and  $\Delta_1 > 0$ , so there are two positive roots for the first equation of (6):

$$I_{11} = \frac{-a_{12} - \sqrt{\Delta_1}}{2a_{11}}, \quad I_{12} = \frac{-a_{12} + \sqrt{\Delta_1}}{2a_{11}}.$$

Direct calculation yields

$$0 < I_{11} < I_{12} < \frac{\beta - \gamma - d}{\beta},$$

so

$$S_{M_{1i}} = \frac{\beta - \gamma - d - \beta I_{1i}}{\beta(1 - \theta)} > 0, \quad i = 1, 2.$$

Thus there exist two endemic equilibria,  $E_{11} = (S_{M_{11}}, I_{11})$  and  $E_{12} = (S_{M_{12}}, I_{12})$ , for Subsystem  $S_{G_1}$ .

If  $R_{c1} = 1$ , we get  $a_{12} < 0$  and  $\Delta_1 = 0$ , so a unique positive root  $I_1 = \frac{-a_{12}}{2a_{11}}$  exists for the first equation of (6). Since  $0 < I_1 < \frac{\beta - \gamma - d}{\beta}$ , it follows that

$$S_{M_1} = \frac{\beta - \gamma - d - \beta I_1}{\beta(1 - \theta)} > 0.$$

Thus a unique endemic equilibrium  $E_1 = (S_{M_1}, I_1)$  exists for Subsystem  $S_{G_1}$ . If  $R_{c1} < 1$ , no positive root exists for equation (6), which suggests no endemic equilibrium exists for Subsystem  $S_{G_1}$ .

We next perform a bifurcation analysis of Subsystem  $S_{G_1}$  at  $\mathcal{R}_0 = 1$ , choosing  $\beta$  as the bifurcation parameter. We have the following results.

**Theorem 1** *The free subsystem undergoes a forward bifurcation at  $\mathcal{R}_0 = 1$  if  $a'_1 < 0$ ; otherwise, it undergoes a backward bifurcation at  $\mathcal{R}_0 = 1$  if  $a'_1 > 0$ , where*

$$a'_1 = (d + \gamma) \frac{2\lambda(1 - \theta)(\theta\lambda + \mu + d + \theta(d + \gamma)) - (\lambda + \mu + d)(\theta\lambda + \mu + d)}{(\theta\lambda + \mu + d)^2}.$$

**Proof** Solving  $\mathcal{R}_0 = 1$  with respect to  $\beta$ , we find the critical value to be

$$\beta^* = \frac{(\lambda + \mu + d)(d + \gamma)}{\theta\lambda + d + \mu}.$$

The right-hand side of the subsystem  $S_{G_1}$  takes the form

$$\begin{aligned} f_{11}(S_M, I) &= \lambda(1 - I) - (\lambda + \mu + d)S_M - \beta\theta S_M I, \\ f_{12}(S_M, I) &= (\beta - \gamma - d)I - \beta(1 - \theta)S_M I - \beta I^2. \end{aligned}$$

The Jacobian matrix of subsystem  $S_{G_1}$  is

$$J_1(S_M, I) = \begin{pmatrix} -(\lambda + \mu + d) - \beta\theta I & -\lambda - \beta\theta S_M \\ -\beta(1 - \theta)I & (\beta - \gamma - d) - \beta(1 - \theta)S_M - 2\beta I \end{pmatrix}.$$

Evaluating this matrix at  $E_0$  and letting  $\beta = \beta^*$  yields

$$J_1(E_0) \Big|_{\beta=\beta^*} = \begin{pmatrix} -(\lambda + \mu + d) & -\lambda & -\frac{\theta\lambda(d+\gamma)}{\theta\lambda+\mu+d} \\ 0 & 0 & 0 \end{pmatrix}.$$

The eigenvalues are  $-\lambda - \mu - d$  and 0, and the left and right eigenvectors corresponding to the eigenvalue 0 are given by

$$u_l = (u_1^l, u_2^l) = (0, 1) \text{ and } u_r = (u_1^r, u_2^r)^T = \left( -\frac{\lambda(\theta\lambda + \mu + d) + \theta\lambda(d + \gamma)}{(\theta\lambda + \mu + d)(\lambda + \mu + d)}, 1 \right)^T.$$

Calculating the nonzero second-order partial derivatives of  $f_{11}$  and  $f_{12}$  at  $(E_0, \beta^*)$ , we get

$$\frac{\partial^2 f_{12}}{\partial S_M \partial I} = \frac{\partial^2 f_{12}}{\partial I \partial S_M} = -\beta^*(1 - \theta), \quad \frac{\partial^2 f_{12}}{\partial I^2} = -\beta^*, \quad \frac{\partial^2 f_{12}}{\partial I \partial \beta} = \frac{\theta\lambda + \mu + d}{\lambda + \mu + d}.$$

Using the results from Castillo-Chavez and Song (2004), we now calculate the two bifurcation parameters

$$a'_1 = \sum_{k,i,j=1}^2 u_k^l u_i^r u_j^r \frac{\partial^2 f_{1k}}{\partial x_i \partial x_j} (E_0, \beta^*) \text{ and } b'_1 = \sum_{k,i=1}^2 u_k^l u_i^r \frac{\partial^2 f_{1k}}{\partial x_i \partial \beta} (E_0, \beta^*),$$

where  $x_i \in \{S_M, I\}$ . We have

$$a'_1 = (d + \gamma) \frac{2\lambda(1 - \theta)(\theta\lambda + \mu + d + \theta(d + \gamma)) - (\lambda + \mu + d)(\theta\lambda + \mu + d)}{(\theta\lambda + \mu + d)^2},$$

$$b'_1 = \frac{\theta\lambda + \mu + d}{\lambda + \mu + d} > 0.$$

If  $a'_1 < 0$ , then a forward bifurcation occurs for the free subsystem at  $\mathcal{R}_0 = 1$ . Otherwise, if  $a'_1 > 0$ , a backward bifurcation occurs for the free subsystem at  $\mathcal{R}_0 = 1$ , as shown in Fig. 2. The parameter values presented in our figures are chosen for illustrative purposes.  $\square$

We next examine the stability of the equilibria. Evaluating  $J_1$  at the disease-free equilibrium  $E_0$  yields

$$\text{tr}(J_1(E_0)) = -(\lambda + \mu + d) - \frac{a_{13}}{\lambda + \mu + d}, \quad \det(J_1(E_0)) = a_{13}.$$

Since  $a_{13} > 0$  for  $\mathcal{R}_0 < 1$ , we get  $\text{tr}(J_1(E_0)) < 0$  and  $\det(J_1(E_0)) > 0$ . It follows that the disease-free equilibrium  $E_0$  is always locally asymptotically stable. We similarly get  $a_{13} < 0$  for  $\mathcal{R}_0 > 1$ , suggesting that  $\det(J_1(E_0)) < 0$ , so the disease-free equilibrium is unstable for  $\mathcal{R}_0 > 1$ .

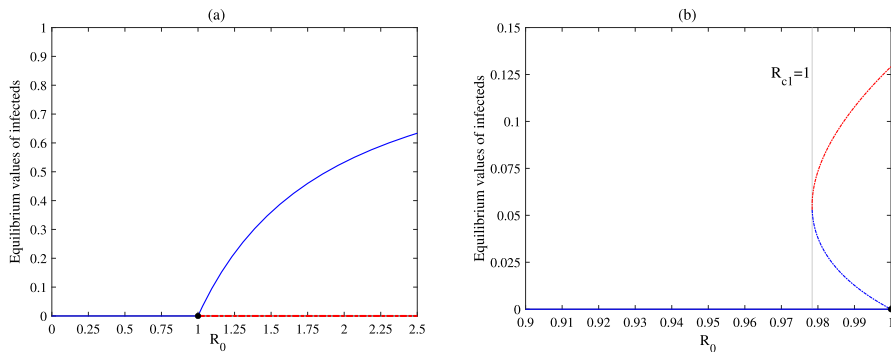


**Fig. 2** (a) Forward bifurcation diagram of the free subsystem. (b) Backward bifurcation diagram of the free subsystem. Here we fix all other parameters as follows:  $\gamma = 0.3, d = 0.008, \theta = 0.5$  and (a)  $\mu = 0.3, \lambda = 0.2$ ; (b)  $\mu = 0.01, \lambda = 0.02$

Next, we analyze the stability of the endemic equilibrium. Calculating the value of the Jacobian matrix  $J_1$  at  $E_{11}$ ,  $E_{12}$  and  $E_1$  gives

$$\begin{aligned} \text{tr}(J_1(E_{11})) &= -(\lambda + \mu + d) - \beta(1 + \theta)I_{11} < 0, & \det(J_1(E_{11})) &= -\sqrt{\Delta_1}I_{11} < 0, \\ \text{tr}(J_1(E_{12})) &= -(\lambda + \mu + d) - \beta(1 + \theta)I_{12} < 0, & \det(J_1(E_{12})) &= \sqrt{\Delta_1}I_{12} > 0, \\ \text{tr}(J_1(E_1)) &= -(\lambda + \mu + d) - \beta(1 + \theta)I_1 < 0, & \det(J_1(E_1)) &= 0. \end{aligned}$$

It follows that the endemic equilibrium  $E_{11}$  is a saddle point, so it is always unstable. The endemic equilibrium  $E_{12}$  is a stable focus for  $\delta_1 < 0$  and a stable node for  $\delta_1 \geq 0$ , where

$$\delta_1 = [(\lambda + \mu + d) + \beta I_{12}(1 + \theta)]^2 - 4 \det(J_1(S_{M12}, I_{12})).$$

The endemic equilibrium  $E_1$  is a non-hyperbolic saddle node. It is crucial to highlight that when the basic reproduction number  $\mathcal{R}_0 < 1$ , the disease does not necessarily vanish. In such cases, another threshold, denoted  $R_{c1}$ , becomes relevant. When  $R_{c1} > 1$ , the disease becomes endemic; conversely, when  $R_{c1} < 1$ , the disease can be eradicated from the population. This underscores the significance of  $R_{c1}$  as a critical threshold for determining whether a disease can be eliminated when  $\mathcal{R}_0 < 1$ . For clarity, we summarize the stability of all the equilibria in Table 2.

### 3.2 Dynamics of the control system

For Subsystem  $S_{G_2}$ , the basic reproduction number is also

$$\mathcal{R}_0 = \frac{\beta(\theta\lambda + d + \mu)}{(\lambda + \mu + d)(d + \gamma)}$$

**Table 2** Existence and stability of all equilibria for Subsystem  $S_{G_1}$ 

The conditions	Equilibria	Stability
$\mathcal{R}_0 > 1$	$E_0$	Unstable
	$E_{12}$	Stable
$\mathcal{R}_0 < 1$	$R_{c1} < 1$ $E_0$	Stable
	$R_{c1} = 1$ $E_0$	Stable
	$E_1$	Unstable
	$R_{c1} > 1$ $E_0$	Stable
	$E_{11}$	Unstable
	$E_{12}$	Stable

and the disease-free equilibrium  $E_0 = (\frac{\lambda}{\lambda + \mu + d}, 0)$  always exists. Denote

$$a_{21} = a_{11} + \beta k(\mu + d), \quad a_{22} = a_{12} + k(a_{13} + \beta \lambda \theta), \quad a_{23} = a_{13}.$$

Then the endemic equilibrium satisfies

$$\begin{aligned} g_2(I) &= a_{21}I^2 + a_{22}I + a_{23} = 0, \\ S_M &= \frac{(\beta - \gamma - d - \beta I)(1 + kI)}{\beta(1 + kI - \theta)}. \end{aligned} \quad (7)$$

If  $\mathcal{R}_0 > 1$ , we have  $a_{21} > 0$ ,  $a_{23} < 0$ , so there is a unique positive root

$$I_{22} = \frac{-a_{22} + \sqrt{\Delta_2}}{2a_{21}}$$

for the first equation of (7), where  $\Delta_2 = a_{22}^2 - 4a_{21}a_{23}$ . Direct calculation yields that  $g_2\left(\frac{\beta - \gamma - d}{\beta}\right) > 0$ , so we have

$$0 < I_{22} < \frac{\beta - \gamma - d}{\beta}.$$

It follows that there is a unique endemic equilibrium  $E_{22} = (S_{M22}, I_{22})$  for Subsystem  $S_{G_2}$ , where

$$S_{M22} = \frac{(\beta - \gamma - d - \beta I_{22})(1 + kI_{22})}{\beta(1 + kI_{22} - \theta)} > 0.$$

If  $\mathcal{R}_0 < 1$ , we can get that  $a_{21} > 0$ ,  $a_{23} > 0$ , so the existence of positive root of (7) depends on the sign of  $a_{22}$  and  $\Delta_2$ . Denote

$$R_{c2} = \frac{\beta\theta(\beta - \gamma - d)}{2\sqrt{a_{21}a_{23}} + a_{22} + \beta\theta(\beta - \gamma - d)}.$$

If  $R_{c2} > 1$ , we have  $a_{22} < 0$ ,  $\Delta_2 > 0$ , so there are two positive roots for the first equation of (7):

$$I_{21} = \frac{-a_{22} - \sqrt{\Delta_2}}{2a_{21}}, \quad I_{22} = \frac{-a_{22} + \sqrt{\Delta_2}}{2a_{21}}.$$

It follows from

$$0 < I_{21} < I_{22} < \frac{\beta - \gamma - d}{\beta}$$

that

$$S_{M2j} = \frac{(\beta - \gamma - d - \beta I_{2j})(1 + kI_{2j})}{\beta(1 + kI_{2j} - \theta)} > 0, \quad j = 1, 2,$$

so there are two endemic equilibria  $E_{21} = (S_{M21}, I_{21})$  and  $E_{22} = (S_{M22}, I_{22})$  for Subsystem  $S_{G_2}$ .

If  $R_{c2} = 1$ , we have  $a_{22} < 0$ ,  $\Delta_2 = 0$ , so only one positive root  $I_2 = \frac{-a_{22}}{2a_{21}}$  exists for the first equation of (7). Since  $0 < I_2 < \frac{\beta - \gamma - d}{\beta}$ , we have

$$S_{M2} = \frac{(\beta - \gamma - d - \beta I_2)(1 + kI_2)}{\beta(1 + kI_2 - \theta)} > 0.$$

Then there is only one endemic equilibrium  $E_2 = (S_{M2}, I_2)$  for Subsystem  $S_{G_2}$ . If  $R_{c2} < 1$ , no positive solution exists for the first equation of (7) and so no endemic equilibrium exists for Subsystem  $S_{G_2}$ .

We next perform a bifurcation analysis for the control subsystem at  $\mathcal{R}_0 = 1$ . By choosing  $\beta$  as the bifurcation parameter and performing a similar procedure to that in Theorem 1, we can show that both a forward and a backward bifurcation are possible for the control subsystem, as shown in Fig. 3.

**Theorem 2** *The control subsystem undergoes a forward bifurcation at  $\mathcal{R}_0 = 1$  for  $\tilde{a} < 0$ ; otherwise, it undergoes a backward bifurcation at  $\mathcal{R}_0 = 1$  for  $\tilde{a} > 0$ , where*

$$\tilde{a} = (d + \gamma) \frac{2\lambda(1 - \theta)(\theta\lambda + \mu + d + \theta(d + \gamma)) - (2k\theta\lambda + \lambda + \mu + d)(\theta\lambda + \mu + d)}{(\theta\lambda + \mu + d)^2}.$$

The proof is given in the appendix.

To explore the stability of the equilibria for the subsystem  $S_{G_2}$ , we first compute the Jacobian matrix of Subsystem  $S_{G_2}$ , matrix  $J_2$ , at  $E_0$  and get

$$\begin{aligned} \text{tr}(J_2(E_0)) &= -(\lambda + \mu + d) - \frac{a_{23}}{\lambda + \mu + d}, \\ \det(J_2(E_0)) &= a_{23}. \end{aligned}$$

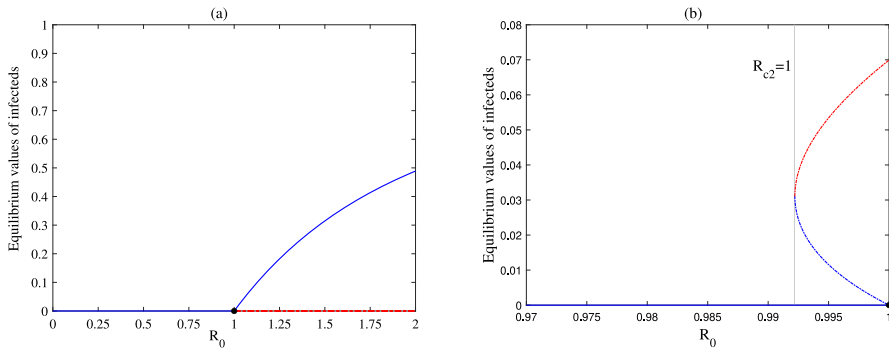


**Fig. 3** (a) Forward bifurcation diagram of the control subsystem. (b) Backward bifurcation diagram of the control subsystem. Here we fix all other parameters as follows:  $\gamma = 0.3$ ,  $d = 0.008$ ,  $\theta = 0.5$ ,  $k = 1.1$  and (a)  $\mu = 0.3$ ,  $\lambda = 0.2$ ; (b)  $\mu = 0.01$ ,  $\lambda = 0.02$

It follows that  $\text{tr}(J_2(E_0)) < 0$  while  $\det(J_2(E_0)) > 0$  for  $\mathcal{R}_0 < 1$ , and  $\det(J_2(E_0)) < 0$  for  $\mathcal{R}_0 > 1$ , so the disease-free equilibrium  $E_0$  is locally asymptotically stable for  $\mathcal{R}_0 < 1$ , and it is unstable for  $\mathcal{R}_0 > 1$ .

Next, we analyze the stability of the endemic equilibria. We have

$$\begin{aligned} \text{tr}(J_2(E_{21})) &= -(\lambda + \mu + d) - \beta I_{21} \left( 1 + \frac{\theta}{1 + k I_{21}} + \frac{\theta k S_{M21}}{(1 + k I_{21})^2} \right) < 0, \\ \det(J_2(E_{21})) &= -\frac{\sqrt{\Delta_2} I_{21}}{1 + k I_{21}} < 0, \\ \text{tr}(J_2(E_{22})) &= -(\lambda + \mu + d) - \beta I_{22} \left( 1 + \frac{\theta}{1 + k I_{22}} + \frac{\theta k S_{M22}}{(1 + k I_{22})^2} \right) < 0, \\ \det(J_2(E_{22})) &= \frac{\sqrt{\Delta_2} I_{22}}{1 + k I_{22}} > 0, \\ \text{tr}(J_2(E_2)) &= -(\lambda + \mu + d) - \beta I_2 \left( 1 + \frac{\theta}{1 + k I_2} + \frac{\theta k S_{M2}}{(1 + k I_2)^2} \right) < 0, \\ \det(J_2(E_2)) &= 0. \end{aligned}$$

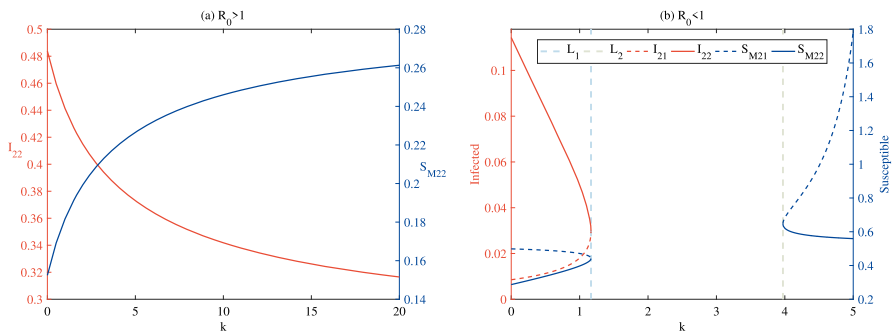
It follows that the endemic equilibrium  $E_{22} = (S_{M22}, I_{22})$  is locally asymptotically stable if  $\mathcal{R}_0 > 1$ . Denote

$$\delta_2 = \left[ (\lambda + \mu + d) + \beta I \left( 1 + \frac{\theta}{1 + k I} + \frac{k \theta S_M}{(1 + k I)^2} \right) \right]^2 - 4 \det(J_2(S_M, I)),$$

so it follows that  $E_{22}$  is a stable focus for  $\delta_2 < 0$  while it is a stable node for  $\delta_2 \geq 0$ . The endemic equilibrium  $E_{21}$  is a saddle point, so it is always unstable. The endemic equilibrium  $E_2$  is a non-hyperbolic saddle node. Once again, in the context of control systems,  $\mathcal{R}_0 < 1$  may not be a sufficient condition for disease extinction. Instead, another threshold,  $R_{c2}$ , must be considered. Only when  $R_{c2} < 1$  can the disease

**Table 3** Existence and stability of all the equilibria for Subsystem  $S_{G_2}$ .

The conditions		Equilibria	Stability
$\mathcal{R}_0 > 1$		$E_0$	Unstable
		$E_{22}$	Stable
$\mathcal{R}_0 < 1$	$R_{c2} < 1$	$E_0$	Stable
		$E_2$	Unstable
	$R_{c2} = 1$	$E_0$	Stable
		$E_{21}$	Unstable
	$R_{c2} > 1$	$E_0$	Stable
		$E_{22}$	Stable

**Fig. 4** Evolution of the equilibrium values of infecteds and social-distancing susceptibles with respect to the social-distancing reinforcement factor  $k$ . Here we fix all other parameters as follows: (a)  $\beta = 0.7$ ,  $\mu = 0.3$ ,  $\lambda = 0.2$ ,  $\gamma = 0.3$ ,  $d = 0.008$ ,  $\theta = 0.5$ ; (b)  $\beta = 0.415$ ,  $\mu = 0.01$ ,  $\lambda = 0.02$ ,  $\gamma = 0.3$ ,  $d = 0.008$ ,  $\theta = 0.5$ 

be effectively eradicated from the population. We summarize the stability of all the equilibria in Table 3.

Due to the significance of the social-distancing reinforcement factor,  $k$ , on the control of disease, it is essential to examine the impact of  $k$  on disease infection. To this purpose, we numerically simulate the effect of varying  $k$  on the equilibrium level of infected individuals and social-distancing susceptibles for Subsystem  $S_{G_2}$ , as shown in Fig. 4.

In Fig. 4, the purple solid (dashed) lines represent the proportion of infected individuals with high (low) endemicity in steady states; i.e.,  $I_{22}$  ( $I_{21}$ ). The pink solid (dashed) lines represent the proportion of social-distancing susceptibles with high (low) endemicity in steady states; i.e.,  $S_{M22}$  ( $S_{M21}$ ). Solving  $R_{c2} = 1$  with respect to  $k$  yields

$$k_{1,2} = \frac{4a_{13}\beta(\mu+d) - 2a_{12}(a_{13} + \beta\lambda\theta) \mp \sqrt{[4a_{13}\beta(\mu+d) - 2a_{12}(a_{13} + \beta\lambda\theta)]^2 - 4(a_{13} + \beta\lambda\theta)(a_{12}^2 - 4a_{11}a_{13})}}{2(a_{13} + \beta\lambda\theta)^2}.$$



Denote

$$L_1 : k = k_1, \quad L_2 : k = k_2.$$

It follows from Fig. 4(a) that the infecteds in the steady state ( $I_{22}$ ) decrease while the social-distancing susceptibles ( $S_{M22}$ ) increase as the social-distancing reinforcement factor increases for  $\mathcal{R}_0 > 1$ . Fig. 4(b) shows that if  $\mathcal{R}_0 < 1$ , there are two endemic equilibria if and only if  $k < k_1$ , while no endemic equilibrium exists if  $k > k_1$ . In fact, no equilibrium exists for (7) for  $k_1 < k < k_2$ ; when  $k \geq k_2$ , the roots for the first equation of (7) are negative, although the roots for the second equation are positive. The infecteds with high endemicity in steady state (i.e.,  $I_{22}$ ) are decreasing, while the ones with low endemicity in steady states (i.e.,  $I_{21}$ ) are increasing as  $k$  increases. Conversely, the social-distancing susceptibles with high endemicity in steady states (i.e.,  $S_{M22}$ ) are increasing, while the ones with low endemicity in steady states (i.e.,  $S_{M21}$ ) are decreasing as  $k$  increases.

#### 4 Sliding domain and its dynamics

In this section, we study the sliding-mode dynamics of system (4) on the switching line  $\Sigma$ . We initially examine the sliding domain, which might exist if the vector of the two subsystems are directed towards each other; i.e.,

$$H(Z) = \langle \sigma_Z(Z), F_{G_1}(Z) \rangle \langle \sigma_Z(Z), F_{G_2}(Z) \rangle < 0.$$

We obtain the sliding domain

$$\Sigma_s = \left\{ (S_M, I) \in R_+^2 \left| \frac{(\beta - \gamma - d - \beta I_c)(1 + k I_c)}{\beta(1 + k I_c - \theta)} \leq S_M \leq \frac{\beta - \gamma - d - \beta I_c}{\beta(1 - \theta)}, I = I_c \right. \right\}$$

when  $I_c < \frac{\beta - \gamma - d}{\beta}$ . Then the crossing region takes the following form:

$$\Sigma_c = \left\{ (S_M, I) \in R_+^2 \left| S_M < \frac{(\beta - \gamma - d - \beta I_c)(1 + k I_c)}{\beta(1 + k I_c - \theta)} \text{ or } S_M > \frac{\beta - \gamma - d - \beta I_c}{\beta(1 - \theta)}, I = I_c \right. \right\}.$$

Using the Filippov convex method, we obtain the sliding dynamics equation of system (4) on the sliding domain  $\Sigma_s$  as follows:

$$\begin{aligned} \frac{dS_M}{dt} &= \lambda(1 - I_c) + (\beta - \gamma - d)I_c - \beta I_c^2 - (\lambda + \mu + d + \beta I_c)S_M, \\ \frac{dI}{dt} &= 0, \end{aligned} \quad (8)$$

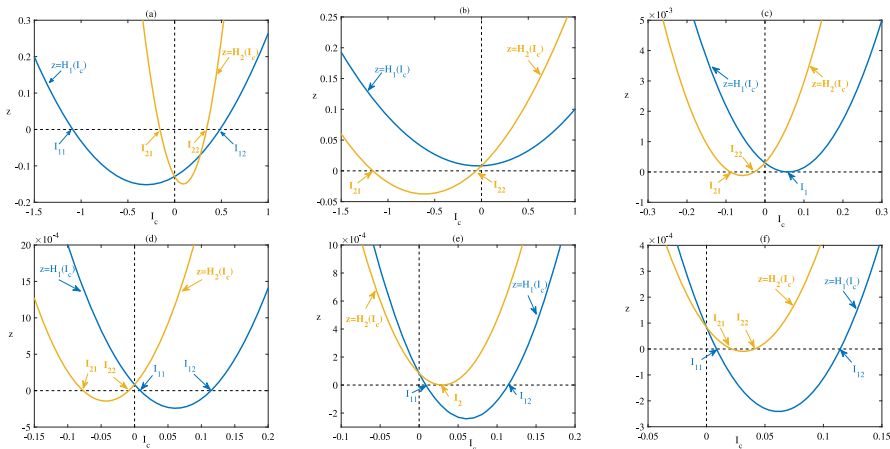


**Fig. 5** The roots of  $H_1(I_c) = 0$  and  $H_2(I_c) = 0$ . (a)  $\beta = 0.7, \mu = 0.3, \gamma = 0.3, d = 0.008, \theta = 0.5, \lambda = 0.2, k = 10$ ; (b)–(f)  $\beta = 0.145, \mu = 0.01, \gamma = 0.3, d = 0.008, \theta = 0.5$  and  $\lambda = 0.1, k = 5$  (b);  $\lambda = 0.22134, k = 5$  (c);  $\lambda = 0.02, k = 5$  (d);  $\lambda = 0.02, k = 1.1663$  (e);  $\lambda = 0.02, k = 1.1$  (f)

with  $S_M \in \Sigma_s$ . For convenience, we denote the sliding vector field as  $F_s$  and the crossing vector field as  $F_c$ . There is a unique equilibrium

$$E_s = (S_{M_s}, I_c) = \left( \frac{\lambda(1 - I_c) + (\beta - \gamma - d)I_c - \beta I_c^2}{\lambda + \mu + d + \beta I_c}, I_c \right)$$

for system (8), so a unique pseudo-equilibrium  $E_s$  exists for Filippov system (4). The pseudo-equilibrium  $E_s$  is admissible if and only if

$$\frac{(\beta - \gamma - d - \beta I_c)(1 + k I_c)}{\beta(1 + k I_c - \theta)} < S_{M_s} < \frac{\beta - \gamma - d - \beta I_c}{\beta(1 - \theta)};$$

i.e.,  $E_s \in \Sigma_s$ , which is equivalent to

$$\begin{aligned} H_1(I_c) &\equiv a_{11}I_c^2 + a_{12}I_c + a_{13} \leq 0, \\ H_2(I_c) &\equiv a_{21}I_c^2 + a_{22}I_c + a_{23} \geq 0. \end{aligned} \quad (9)$$

We next discuss the solution of the inequalities (9).

When  $\mathcal{R}_0 > 1$ , we have  $a_{11} > 0$  and  $a_{13} < 0$ , so it follows that the solutions for  $H_1(I_c) = 0$  are  $I_c = I_{11}$  and  $I_c = I_{12}$  with  $I_{11} < 0 < I_{12}$ . We similarly have  $a_{21} > 0$  and  $a_{23} < 0$ , so there are two solutions,  $I_c = I_{21}$  and  $I_c = I_{22}$ , for  $H_2(I_c) = 0$  with  $I_{21} < 0 < I_{22}$ . Since  $I_{11} < I_{21} < I_{22} < I_{12}$ , the solution for (9) is  $I_{22} \leq I_c \leq I_{12}$ , as shown in Fig. 5(a). Thus the pseudo-equilibrium  $E_s$  is admissible for  $I_{22} \leq I_c \leq I_{12}$  in this scenario.

When  $\mathcal{R}_0 < 1$ , the solution of (9) depends on the positive solutions to the equations  $H_1(I_c) = 0$  and  $H_2(I_c) = 0$ , which depends on whether the threshold value  $R_{cj}$  ( $j =$

**Table 4** Existence of the admissible pseudo-equilibrium  $E_s$  for Filippov system (4)

Parameter values $\mathcal{R}_0 > 1$	Ranges of threshold $I_{22} \leq I_c \leq I_{12}$	Admissible/Virtual Admissible
$\mathcal{R}_0 < 1$		
$R_{c1} < 1$		Virtual
$R_{c1} = 1$	$I_c = I_1$	Admissible
$R_{c2} \leq 1 < R_{c1}$	$I_{11} \leq I_c \leq I_{12}$	Admissible
$R_{c2} > 1$	$I_{11} \leq I_c \leq I_{21}$ or $I_{22} \leq I_c \leq I_{12}$	Admissible

1, 2) is greater or less than 1. We know  $R_{c1} > R_{c2}$ , and there are further three possibilities to consider according to the relationship of  $R_{c1}$ ,  $R_{c2}$  and 1.

If  $R_{c1} < 1$ , no positive solution exists for  $H_1(I_c) = 0$  or  $H_2(I_c) = 0$ , as shown in Fig. 5(b), so no solution exists for the inequalities (9). Hence, the pseudo-equilibrium  $E_s$  is virtual for Filippov system (4) in this scenario.

If  $R_{c1} = 1$ , there is no positive solution for  $H_1(I_c) = 0$  while a unique positive solution  $I_c = I_2$  for  $H_2(I_c) = 0$ , as shown in Fig. 5(c), so the solution for the inequalities (9) is  $I_c = I_1$ . Hence, the pseudo-equilibrium  $E_s$  is admissible for  $I_c = I_1$  in this scenario.

If  $R_{c2} < 1 < R_{c1}$ , there are two positive solutions,  $I_{11}$  and  $I_{12}$ , for the equation  $H_1(I_c) = 0$ , but no positive solution exists for  $H_2(I_c) = 0$ , so the solution for the inequalities (9) is  $I_{11} < I_c \leq I_{12}$ , as shown in Fig. 5(d). Thus the pseudo-equilibrium  $E_s$  is admissible in this range.

If  $R_{c2} = 1 < R_{c1}$ , two positive solutions,  $I_{11}$  and  $I_{12}$ , exist for  $H_1(I_c) = 0$ , and one positive solution,  $I_2$ , exists for  $H_2(I_c) = 0$ . Since  $I_{11} < I_2 < I_{12}$ , the solution for the inequalities (9) is  $I_{11} \leq I_c \leq I_{12}$ , as shown in Fig. 5(e). Thus, the pseudo-equilibrium  $E_s$  is admissible for  $I_{11} \leq I_c \leq I_{12}$  in this scenario.

If  $R_{c2} > 1$ , similar analysis yields that the solutions for the inequalities (9) are  $I_{11} < I_c < I_{21}$  and  $I_{22} < I_c < I_{12}$ , as shown in Fig. 5(f). Hence the pseudo-equilibrium  $E_s$  is admissible for the Filippov system (4) for  $I_{11} < I_c < I_{21}$  or  $I_{22} < I_c < I_{12}$ .

For clarity, we summarize the conditions to ensure the pseudo-equilibrium  $E_s$  is admissible in Table 4.

Considering the importance of the social-distancing reinforcement factor on the transmission of epidemic disease, we numerically investigate how the sliding mode and equilibria change as the parameter  $k$  varies, as shown in Fig. 6. The yellow stars represent the endemic equilibria of Subsystem  $S_{G1}$ , the triangles denote the endemic equilibria of Subsystem  $S_{G2}$  with higher endemicity (shown in Fig. 6(a)), and the squares represent the pseudo-equilibria (shown in Fig. 6(a),(b)). The solid shapes represent real/admissible equilibria, while the hollow shapes represent virtual equilibria.

Figure 6 shows that the sliding-mode region enlarges as the parameter  $k$  increases for both  $\mathcal{R}_0 > 1$  and  $\mathcal{R}_0 < 1$ . When  $\mathcal{R}_0 > 1$ , Fig. 6(a) indicates that two endemic equilibria coexist for Subsystem (4), one for Subsystem  $S_{G1}$  (the yellow stars,  $E_{12}$ ) and the other for Subsystem  $S_{G2}$  (the yellow triangles,  $E_{22}$ ). Further,  $E_{12}$  is real and independent of  $k$  while a real/virtual bifurcation occurs at  $E_{22}$  when the parameter  $k$

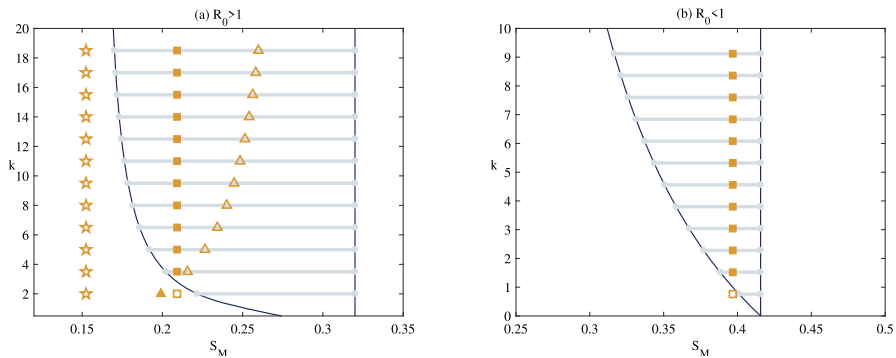


**Fig. 6** Evolution of the sliding modes (grey thick solid lines), the regular endemic equilibria (yellow stars and triangles) and pseudo-equilibria (yellow squares) for Filippov system (4) with respect to the reinforcement factor of social-distancing  $k$ . Here we fix all other parameters as follows: (a)  $\beta = 0.7, \mu = 0.3, \lambda = 0.2, \gamma = 0.3, d = 0.008, \theta = 0.5$ ; (b)  $\beta = 0.415, \mu = 0.01, \lambda = 0.02, \gamma = 0.3, d = 0.008, \theta = 0.5$

passes through a critical value around  $c = 3$ , where the admissible pseudo-equilibrium  $E_s$  appears. When  $\mathcal{R}_0 < 1$ , Fig. 6(b) demonstrates that the pseudo-equilibrium  $E_s$  is admissible when  $k$  is greater than the critical value around  $k = 1.5$ .

## 5 Boundary equilibrium bifurcation

In this section, we study the bifurcation phenomenon of equilibria in Filippov system (4). We initially investigate whether the endemic equilibria of Filippov system (4) are real or virtual. It follows from Section 3 that there are six possible endemic equilibria for Filippov system (4):  $E_{11}, E_{12}, E_{21}, E_{22}, E_1$  and  $E_2$ . As the threshold value  $I_c$  changes, they may be real or virtual. In particular,  $E_{11}, E_{21}, E_1$  are real, denoted as  $E_{11}^r, E_{21}^r, E_1^r$ , if  $I_c > I_{11}, I_c > I_{12}$  and  $I_c > I_1$ , respectively; they are virtual, denoted as  $E_{11}^v, E_{21}^v, E_1^v$ , if  $I_c < I_{11}, I_c < I_{12}$  and  $I_c < I_1$ , respectively. The endemic equilibria  $E_{21}, E_{22}, E_2$  are real, denoted as  $E_{21}^r, E_{22}^r, E_2^r$ , if  $I_c < I_{21}, I_c < I_{22}$  and  $I_c < I_2$ , respectively; they are virtual, denoted as  $E_{21}^v, E_{22}^v, E_2^v$ , if  $I_c > I_{21}, I_c > I_{12}$  and  $I_c > I_2$ , respectively.

Next, we examine the tangent points and boundary equilibrium of Filippov system (4). According to Definition 3, the tangent points of Filippov system (4) satisfy

$$(\beta - \gamma - d)I - \beta \left( 1 - \frac{\theta}{1 + vkI} \right) S_M I - \beta I^2 = 0, \quad (10)$$

$$I = I_c.$$

Solving (10), there are two tangent points  $T_1, T_2$  for Filippov system (4),

$$T_1 = \left( \frac{(\beta - \gamma - d - \beta I_c)(1 + kI_c)}{\beta(1 + kI_c - \theta)}, I_c \right) \quad \text{and} \quad T_2 = \left( \frac{\beta - \gamma - d - \beta I_c}{\beta(1 - \theta)}, I_c \right).$$

According to Definition 4, the boundary equilibria of Filippov system (4) satisfy

$$\begin{aligned}\lambda(1 - I - S_M) - \frac{\beta\theta S_M I}{1 + vkI} - (\mu + d)S_M &= 0, \\ (\beta - \gamma - d)I - \beta\left(1 - \frac{\theta}{1 + vkI}\right)S_M I - \beta I^2 &= 0, \\ I &= I_c.\end{aligned}\quad (11)$$

If  $\nu = 0$ , there are three boundary equilibria,

$$\begin{aligned}E_{11}^b &= \left(\frac{\beta - \gamma - d - \beta I_{11}}{\beta(1 - \theta)}, I_{11}\right), \quad E_{12}^b = \left(\frac{\beta - \gamma - d - \beta I_{12}}{\beta(1 - \theta)}, I_{12}\right) \\ \text{and } E_1^b &= \left(\frac{\beta - \gamma - d - \beta I_1}{\beta(1 - \theta)}, I_1\right)\end{aligned}$$

for  $I_{11} = I_c$ ,  $I_{12} = I_c$  or  $I_1 = I_c$ . If  $\nu = 1$ , there are also three boundary equilibria,

$$\begin{aligned}E_{21}^b &= \left(\frac{(\beta - \gamma - d - \beta I_{21})(1 + kI_{21})}{\beta(1 + kI_{21} - \theta)}, I_{21}\right), \\ E_{22}^b &= \left(\frac{(\beta - \gamma - d - \beta I_{22})(1 + kI_{22})}{\beta(1 + kI_{22} - \theta)}, I_{22}\right), \\ E_2^b &= \left(\frac{(\beta - \gamma - d - \beta I_2)(1 + kI_2)}{\beta(1 + kI_2 - \theta)}, I_2\right),\end{aligned}$$

for  $I_{21} = I_c$ ,  $I_{22} = I_c$  or  $I_2 = I_c$ .

By the above discussion, we know that there are six possible boundary equilibria for Filippov system (4). According to Definition 4, if we further have

$$\det(J_1(E_s^b)) \neq 0, \quad \det(J_2(E_s^b)) \neq 0, \quad s \in \{11, 12, 21, 22\},$$

then a boundary equilibrium bifurcation occurs. We initially examine the scenario with  $\mathcal{R}_0 > 1$ . There exists a disease-free equilibrium  $E_0$  and two endemic equilibria  $E_{12}$  and  $E_{22}$  for  $\mathcal{R}_0 > 1$ , where  $E_0$  is unstable. If  $I_c < I_{22}$ , the equilibrium  $E_{22}^r$  is real while the equilibrium  $E_{12}^v$  is virtual, and the sliding mode is as shown in Fig. 7(a).

When  $I_c$  increases to  $I_c = I_{22}$ , the endemic equilibrium  $E_{22}$  and the tangent point  $T_1$  coincide, resulting in the occurrence of a boundary equilibrium  $E_{22}^b$ , so a boundary-node (focus) bifurcation occurs, as shown in Fig. 7(b). When  $I_c$  increases continuously to  $I_c > I_{22}$ , the boundary equilibrium  $E_{22}^b$  disappears, and the pseudo-equilibrium  $E_s$  and virtual equilibrium  $E_{22}^v$  occur, as shown in Fig. 7(c). Similarly, the endemic equilibrium  $E_{12}$ , the tangent point  $T_2$  and the pseudo-equilibrium  $E_s$  coincide for  $I_c = I_{12}$ , so another boundary-node (focus) bifurcation occurs for Filippov system (4). Thus, the following conclusion can be obtained.

**Theorem 3** A boundary-node (focus) bifurcation for Filippov system (4) at the equilibrium  $E_{22}^b$  (resp.,  $E_{12}^b$ ) occurs if  $\det(J_1(E_{22}^b)) \neq 0$  (resp.,  $\det(J_2(E_{12}^b)) \neq 0$ ).

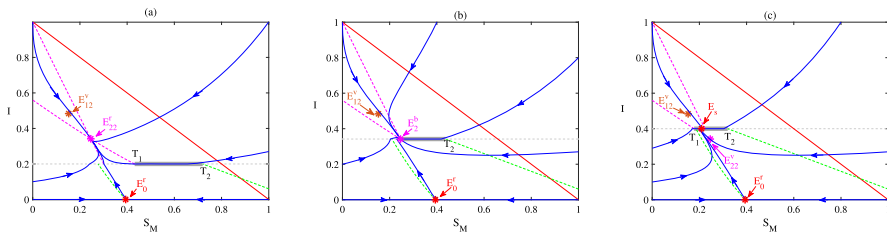


**Fig. 7** Boundary node bifurcation for Filippov system (4). Here we choose  $I_c$  as a bifurcation parameter and all other parameters as follows:  $\beta = 0.7$ ,  $\mu = 0.3$ ,  $\lambda = 0.2$ ,  $\gamma = 0.3$ ,  $d = 0.008$ ,  $\theta = 0.5$  and  $k = 10$ , with (a)  $I_c = 0.2$ ; (b)  $I_c = 0.3418$ ; (c)  $I_c = 0.4$

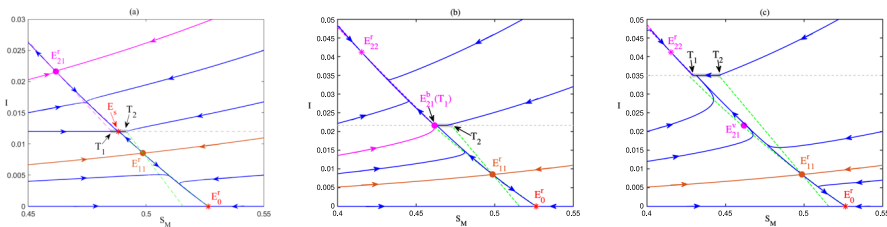


**Fig. 8** Boundary saddle-node bifurcation for Filippov system (4). Here we choose  $I_c$  as a bifurcation parameter, and all other parameters as follows:  $\beta = 0.415$ ,  $\mu = 0.01$ ,  $\lambda = 0.02$ ,  $\gamma = 0.3$ ,  $d = 0.008$ ,  $\theta = 0.5$  and  $k = 1.1$ , with (a)  $I_c = 0.012$ ; (b)  $I_c = 0.0216$ ; (c)  $I_c = 0.035$

Next, we consider the scenario with  $\mathcal{R}_0 < 1$ . In this scenario, there are six possible endemic equilibria  $E_{11}$ ,  $E_{12}$ ,  $E_{21}$ ,  $E_{22}$ ,  $E_1$  and  $E_2$ , where  $E_{11}$  and  $E_{21}$  are saddles,  $E_{12}$  and  $E_{22}$  are nodes or foci and  $E_1$  and  $E_2$  are saddle nodes. If we further have  $R_{c2} > 1$ , there are four endemic equilibria  $E_{11}$ ,  $E_{12}$ ,  $E_{21}$  and  $E_{22}$  of the system (4). When  $I_{11} < I_c < I_{12}$ , the equilibrium  $E_{21}^r$  is real and a saddle, as shown in Fig. 8(a).

If  $I_c$  increases to  $I_c = I_{21}$  (i.e.,  $I_c = 0.0216$ ), the endemic equilibrium  $E_{21}^r$ , the tangent point  $T_1$  and the pseudo-equilibrium  $E_s$  coincide, resulting in the occurrence of the boundary equilibrium  $E_{21}^b$ , as shown in Fig. 8(b). Since the regular equilibrium  $E_{21}^r$  is a saddle and the pseudo-equilibrium  $E_s$  is a pseudo node, the boundary equilibrium  $E_{21}^b$  is a saddle-node. Hence a boundary saddle-node bifurcation occurs for Filippov system (4). If  $I_c$  increases continuously to  $I_c > I_{21}$  (i.e.,  $I_c = 0.035$ ), the boundary equilibrium  $E_{21}^b$  disappears, and a virtual equilibrium  $E_{21}^v$  occurs, as shown in Fig. 8(c). As the threshold  $I_c$  undergoes the following variation

$$I_c < I_{21} \longrightarrow I_c = I_{21} \longrightarrow I_c > I_{21},$$

we obtain the following variation

$$\text{real saddle} \longrightarrow \text{pseudo-saddle-node} \longrightarrow \text{virtual equilibrium}.$$

That is, a saddle-node (the boundary equilibrium  $E_{21}^b$ ) appears as the result of the collision of a regular saddle (i.e., endemic equilibrium  $E_{21}^r$ ) and a pseudo-node (i.e., the pseudo-equilibrium  $E_s$ ), and it finally disappears with the appearance of a virtual equi-

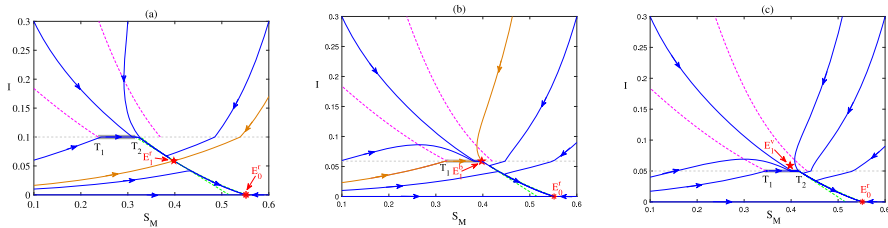


**Fig. 9** Boundary saddle-node bifurcation for Filippov system (4). Here we choose  $I_c$  as a bifurcation parameter and all other parameters as follows:  $\beta = 0.415$ ,  $\mu = 0.01$ ,  $\lambda = 0.022134$ ,  $\gamma = 0.3$ ,  $d = 0.008$ ,  $\theta = 0.5$  and  $k = 5$ , with (a)  $I_c = 0.1$ ; (b)  $I_c = 0.0589$ ; (c)  $I_c = 0.05$ .

librium (i.e.,  $E_{21}^b$ ). This illustrates how a regular saddle becomes a pseudo-saddle-node. The bifurcation induces a novel equilibrium: the pseudo-saddle-node for Filippov system (4). Similarly, we can get another boundary saddle-node bifurcation when the endemic equilibrium  $E_{11}^r$  and the pseudo-equilibrium  $E_s$  coincide. We summarize these results in the following theorem.

**Theorem 4** A boundary saddle-node bifurcation occurs for Filippov system (4) at the equilibrium  $E_{21}^b$  (resp.,  $E_{11}^b$ ) if  $\det(J_1(E_{21}^b)) \neq 0$  (resp.,  $\det(J_2(E_{11}^b)) \neq 0$ ).

When  $\mathcal{R}_0 < 1$  and  $R_{c1} = 1$ , there is an endemic equilibrium  $E_1$  as well as a disease-free equilibrium  $E_0$ . If we further have  $I_c > I_1$ , the equilibrium  $E_1^r$  is real, and it is a saddle-node for Filippov system (4), as shown in Fig. 9(a).

If  $I_c$  decreases to  $I_c = I_1$  (i.e.,  $I_c = 0.0589$ ), the equilibrium  $E_1^r$  and tangent point  $T_2$  collide, leading to a boundary equilibrium  $E_1^b$ , so a boundary saddle-node bifurcation occurs for Filippov system (4), as shown in Fig. 9(b). If  $I_c$  decreases to  $I_c < I_1$  (i.e.,  $I_c = 0.05$ ), the boundary saddle-node disappears with the appearance of a virtual equilibrium  $E_1^v$ , as shown in Fig. 9(c). Note that the boundary saddle-node in Fig. 9 is induced by the collision of a regular saddle-node and a tangent point; while the boundary saddle-node in Fig. 8 is induced by the collision of a regular saddle, a pseudo-node and a tangent point. Similarly, another boundary saddle-node bifurcation occurs when the regular saddle-node  $E_2$  collides with the tangent point  $T_1$ . We summarize these results in the following theorem.

**Theorem 5** A boundary saddle-node bifurcation occurs for Filippov system (4) at the equilibrium  $E_1^b$  (resp.,  $E_2^b$ ) if  $I_c = I_1$  (resp.,  $I_c = I_2$ ).

## 6 Global behaviour of the system

The global behaviour of Filippov system (4) is explored in this section. By examining the nonexistence of all possible limit cycles, we gain insight into the global stability of all equilibria.

## 6.1 Nonexistence of limit cycles

In this section, we address the nonexistence of limit cycles to obtain the global stability of all the equilibria of the system (4). We initially rule out the existence of standard cycles, which lie totally in the subregion  $G_1$  or  $G_2$ .

**Lemma 1** *There is no limit cycle for Filippov system (4) totally in region  $G_i$ ,  $i = 1, 2$ .*

**Proof** Let the Dulac function be  $B = \frac{1}{S_M I}$ . For Subsystem  $S_{G_1}$ , we have

$$\frac{\partial(Bf_{11})}{\partial S_M} + \frac{\partial(Bf_{12})}{\partial I} = \frac{-\lambda(1-I) - \beta S_M I}{S_M^2 I} < 0,$$

so there is no limit cycle totally in region  $G_1$ . Similarly, for Subsystem  $S_{G_2}$ , we have

$$\frac{\partial(Bf_{21})}{\partial S_M} + \frac{\partial(Bf_{22})}{\partial I} = \frac{-\lambda(1-I) - \beta S_M I}{S_M^2 I} - \frac{\beta \theta k}{(1+kI)^2} < 0.$$

Hence there is no limit cycle totally in region  $G_2$ .  $\square$

**Lemma 2** *There is no closed orbit for Filippov system (4) that contains part of the sliding domain  $\Sigma_s$ .*

**Proof** We only preclude the existence of closed orbit containing part of  $\Sigma_s$  for  $\mathcal{R}_0 > 1$ ; a similar process can be implemented for the case  $\mathcal{R}_0 < 1$ . If  $\mathcal{R}_0 > 1$ , the disease-free equilibrium  $E_0$  and endemic equilibria  $E_{11}$ ,  $E_{21}$  exist for Filippov system (4). There are three further possibilities to consider:  $I_{22} \leq I_c \leq I_{12}$ ,  $I_c > I_{12}$  and  $I_c < I_{22}$ . If  $I_{22} \leq I_c \leq I_{12}$ , the pseudo-equilibrium  $E_s$  exists and is asymptotically stable for  $I_{22} < I_c < I_{12}$ , so there is no limit cycle containing part of the sliding domain  $\Sigma_s$ . If  $I_c > I_{12}$ , it follows from the sliding dynamics (8) that  $\frac{dS_M}{dt} > 0$ , which indicates that any trajectory reaching the sliding domain  $\Sigma_s$  moves from left to right on  $\Sigma_s$ . Denote the orbit initiating from the tangent point  $T_2$  as  $l_1$ . We only need to prove that  $l_1$  will not hit the manifold  $\Sigma_s$  again. In fact, since  $E_{21}$  is stable, by a similar process in Wang and Xiao (2014), the orbit  $l_1$  cannot hit the manifold  $\Sigma$ , but rather spirals to the stable equilibrium  $E_{21}$ . Hence there is no closed orbit for Filippov system (4) that contains part of the sliding segment. If  $I_c < I_{22}$ , a similar analysis yields no limit cycle containing part of the sliding domain  $\Sigma_s$ .  $\square$

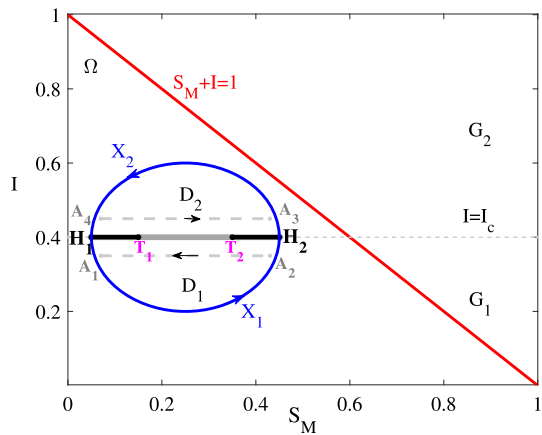
**Lemma 3** *There is no limit cycle surrounding the sliding domain  $\Sigma_s$ .*

**Proof** We apply a similar method as in Xiao et al. (2012) to preclude the existence of a limit cycle surrounding  $\Sigma_s$ . Suppose that  $X$  is a limit cycle surrounding the sliding segment  $T_1 T_2$  with period  $T$ , as shown in Fig. 10.  $\square$

Denote its part below the line  $I = I_c$  by  $X_1$  and its part above the line  $I = I_c$  by  $X_2$ . The intersection points of the limit cycle  $X$  and the line  $I = I_c$  are represented



**Fig. 10** Phase plane  $S_M$ - $I$  for Filippov epidemic model (2), showing the switching line ( $I = I_c$ ), sliding domain ( $T_1T_2$ ) and the diagram of  $X_1$  and  $X_2$  split from the limit cycle by the switching line



by  $H_1$  and  $H_2$ . Plot two auxiliary lines  $I = I_c - \epsilon$  and  $I = I_c + \epsilon$ , where  $\epsilon > 0$  is any sufficiently small number. Denote the intersection points of  $X$  and the auxiliary line  $I = I_c - \epsilon$  by  $A_1$  and  $A_2$ , and the intersection points of  $X$  and another auxiliary line  $I = I_c + \epsilon$  by  $A_4$  and  $A_3$ . Let  $D_1$  be the region delimited by  $X_1$  and the segment  $A_2A_1$ , and let  $D_2$  be the region delimited by  $X_2$  and the segment  $A_4A_3$ . We denote the boundary of  $D_1$  and  $D_2$  by  $C_1$  and  $C_2$ , respectively, with the directions indicated in Fig. 10. Let the Dulac function be  $B = \frac{1}{S_M I}$  defined as before. By the discussion given above and Green's theorem, we get

$$\begin{aligned} \iint_{D_1} \left[ \frac{\partial(Bf_{11})}{\partial S_M} + \frac{\partial(Bf_{12})}{\partial I} \right] dS_M dI &= \oint_{C_1} B [f_{11} dI - f_{12} dS_M] = - \int_{A_2 A_1} B f_{12} dS_M, \\ \iint_{D_2} \left[ \frac{\partial(Bf_{21})}{\partial S_M} + \frac{\partial(Bf_{22})}{\partial I} \right] dS_M dI &= \oint_{C_2} B [f_{21} dI - f_{22} dS] = - \int_{A_4 A_3} B f_{22} dS_M. \end{aligned}$$

Let  $D_0 \subset D_1$  and

$$\xi = \iint_{D_0} \left[ \frac{\partial(Bf_{11})}{\partial S_M} + \frac{\partial(Bf_{12})}{\partial I} \right] dS_M dI.$$

Then

$$\frac{\partial(Bf_{11})}{\partial S_M} + \frac{\partial(Bf_{12})}{\partial I} < 0 \implies \xi < 0.$$

Furthermore,

$$0 > \xi > \iint_{D_1} \left[ \frac{\partial(Bf_{11})}{\partial S_M} + \frac{\partial(Bf_{12})}{\partial I} \right] dS_M dI + \iint_{D_2} \left[ \frac{\partial(Bf_{21})}{\partial S_M} + \frac{\partial(Bf_{22})}{\partial I} \right] dS_M dI,$$

so we obtain

$$0 > \xi > - \int_{A_2 A_1} B f_{12} dS_M - \int_{A_4 A_3} B f_{22} dS_M. \quad (12)$$

Assume that the abscissae of the points  $H_1, H_2, A_1, A_2, A_3, A_4$  are  $\underline{s}, \bar{s}, \underline{s} + h_1(\epsilon), \bar{s} - h_2(\epsilon), \bar{s} - h_3(\epsilon)$  and  $\underline{s} + h_4(\epsilon)$ , respectively, where  $h_i(\epsilon) (i = 1, 2, 3, 4)$  is continuous and satisfies  $\lim_{\epsilon \rightarrow \infty} h_i(\epsilon) = 0$  and  $h_i(\epsilon) = 0$ . Thus, we get

$$\begin{aligned} \lim_{\epsilon \rightarrow \infty} \left[ - \int_{A_2 A_1} B f_{12} dS_M \right] &= \lim_{\epsilon \rightarrow \infty} \int_{\underline{s} + h_1(\epsilon)}^{\bar{s} - h_2(\epsilon)} \left[ \frac{\beta - \gamma - d - \beta(I_c - \epsilon)}{S_M} - \beta(1 - \theta) \right] dS_M \\ &= \lim_{\epsilon \rightarrow \infty} \left[ (\beta - \gamma - d - \beta(I_c - \epsilon)) \ln \left| \frac{\bar{s} - h_2(\epsilon)}{\underline{s} + h_1(\epsilon)} \right| \right. \\ &\quad \left. - \beta(1 - \theta)(\bar{s} - h_2(\epsilon) - \underline{s} - h_1(\epsilon)) \right] \\ &= (\beta - \gamma - d - \beta I_c) \ln \left| \frac{\bar{s}}{\underline{s}} \right| - \beta(1 - \theta)(\bar{s} - \underline{s}). \end{aligned}$$

Similarly, we have

$$\begin{aligned} \lim_{\epsilon \rightarrow \infty} \left[ - \int_{A_4 A_3} B f_{22} dS_M \right] &= \lim_{\epsilon \rightarrow \infty} \int_{\underline{s} + h_4(\epsilon)}^{\bar{s} - h_3(\epsilon)} \left[ \frac{\beta - \gamma - d - \beta(I_c - \epsilon)}{S_M} \right. \\ &\quad \left. - \beta \left( 1 - \frac{\theta}{1 + k(I_c + \epsilon)} \right) \right] dS_M \\ &= \lim_{\epsilon \rightarrow \infty} \left[ (\beta - \gamma - d - \beta(I_c - \epsilon)) \ln \left| \frac{\underline{s} + h_4(\epsilon)}{\bar{s} - h_3(\epsilon)} \right| \right. \\ &\quad \left. - \beta \left( 1 - \frac{\theta}{1 + k(I_c + \epsilon)} \right) (\underline{s} + h_4(\epsilon) - \bar{s} + h_3(\epsilon)) \right] \\ &= (\beta - \gamma - d - \beta I_c) \ln \left| \frac{\underline{s}}{\bar{s}} \right| - \beta \left( 1 - \frac{\theta}{1 + k I_c} \right) (\underline{s} - \bar{s}). \end{aligned}$$

Therefore

$$\lim_{\epsilon \rightarrow \infty} \left[ - \int_{A_2 A_1} B f_{12} dS_M - \int_{A_4 A_3} B f_{22} dS_M \right] = \beta \theta (\bar{s} - \underline{s}) \left( 1 - \frac{1}{1 + k I_c} \right) > 0,$$

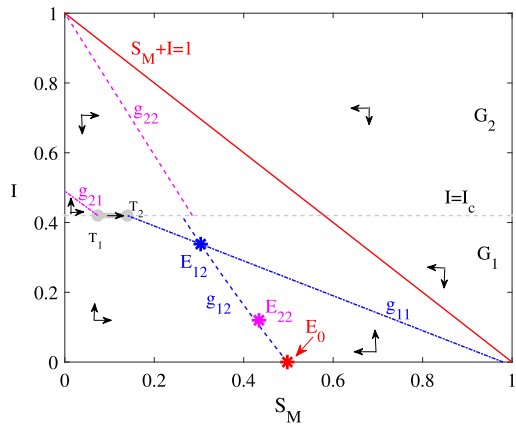
which contradicts (12). Hence, no limit cycle surrounds the sliding domain  $\Sigma_s$ .

**Lemma 4** *There is no crossing cycle without surrounding the sliding domain, which is composed of pieces of the orbit of  $F_{G_1}$ , pieces of the orbit of  $F_{G_2}$  and the orbit of  $F_c$ .*

**Proof** The horizontal and vertical isoclinic curves for the free system are

$$\left\{ (S_M, I) \in R_+^2 \mid S_M = \frac{\lambda(1 - I)}{\lambda + \mu + d + \beta \theta I}, I < I_c \right\}$$

**Fig. 11** Phase plane  $S_M$ - $I$  for Filippov system (4), showing the switching line ( $I = I_c$ ) and the sliding domain ( $T_1 T_2$ ). The horizontal and vertical isoclinic curves for the free system (resp. control system) are  $g_{11}$  and  $g_{12}$  (resp.  $g_{21}$  and  $g_{22}$ )



and

$$\left\{ (S_M, I) \in \mathbb{R}_+^2 \mid I = \frac{\beta - \gamma - d - \beta(1 - \theta)I}{\beta}, I < I_c \right\},$$

respectively, denoted by  $g_{11}$  and  $g_{12}$ . The horizontal and vertical isoclinic curves for the control system are

$$\left\{ (S_M, I) \in \mathbb{R}_+^2 \mid F = \frac{\lambda(1 - I)(1 + kI)}{(\lambda + \mu + d)(1 + kI) + \beta\theta I}, I > I_c \right\}$$

and

$$\left\{ (S_M, I) \in \mathbb{R}_+^2 \mid I = \frac{\beta - \gamma - d}{\beta} - \frac{(1 + kI - \theta)F}{1 + kI}, I > I_c \right\},$$

respectively, denoted by  $g_{21}$  and  $g_{22}$ . The vector field to the right of the null-isoclines  $g_{11}$  and  $g_{21}$  points down and the vector field to the left of the null-isoclines points up, as shown in Fig. 11.  $\square$

Hence there is also no crossing limit cycle.

## 6.2 Global stability

We focus on the global stability of Filippov system (4) based on the above discussion. By Sections 3–4, there are three regular equilibria,  $E_0$ ,  $E_{12}$  and  $E_{22}$ , for  $\mathcal{R}_0 > 1$ , and there is a pseudo-equilibrium state  $E_s$  if and only if  $I_{22} < I_c < I_{12}$  for system (4), as shown in Fig. 5(a). In this scenario, the global behaviour of Filippov system (4) is as follows.

**Theorem 6** *The endemic equilibria  $E_{22}^*$  is globally asymptotically stable for Filippov system (4) if  $I_c < I_{22}$ ; the pseudo-equilibrium  $E_s$  is globally asymptotically stable*

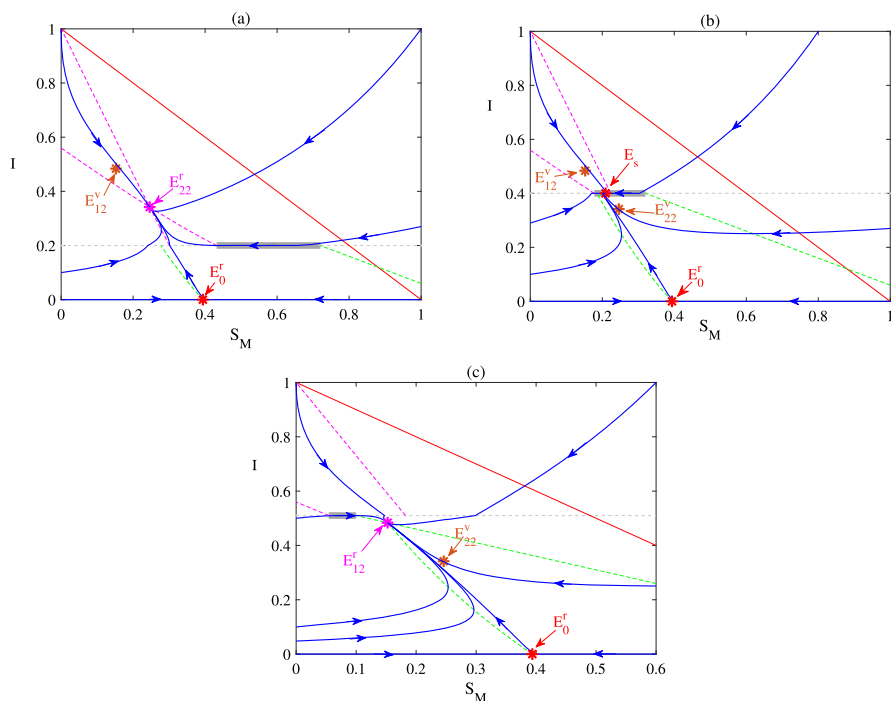


**Fig. 12** Phase plane of Filippov epidemic model (4).  $\beta = 0.7$ ,  $\mu = 0.3$ ,  $\lambda = 0.2$ ,  $\gamma = 0.3$ ,  $d = 0.008$ ,  $\theta = 0.5$  and  $k = 10$ , with (a)  $I_c = 0.2$ ; (b)  $I_c = 0.4$ ; (c)  $I_c = 0.51$ . The pink (resp. orange) asterisks represent the real (resp. virtual) equilibria and the red asterisks represent the disease-free equilibria and pseudo-equilibrium

if  $I_{22} < I_c < I_{12}$ ; the endemic equilibrium  $E_{12}^r$  is globally asymptotically stable if  $I_c > I_{12}$ .

**Proof** By Section 3, the disease-free equilibrium  $E_0^r$  and the endemic equilibrium  $E_{22}^r$  are real for system (4); while the endemic equilibrium  $E_{12}^v$  is virtual when  $I_c < I_{22}$ . The real equilibrium  $E_0^r$  is a saddle, so it is unstable. It follows from Lemmas 1–4 that no limit cycle exists for Filippov system (4). Hence the real equilibrium  $E_{22}^r$  is globally asymptotically stable for  $I_c < I_{22}$ , as shown in Fig. 12(a).  $\square$

In Fig. 12, the thick grey solid lines represent the sliding domains, the thin grey dashed lines represent the crossing regions, the pink, green and red asterisks represent the real, virtual and disease-free equilibria and pseudo-equilibria, the pink (resp. green) dashed curves represent the asymptotes of the control system (resp. free system), and the blue solid curves are the trajectories of Filippov model (4). If  $I_{22} < I_c < I_{12}$ , there is an admissible pseudo-equilibrium  $E_s$  for system (4), and it is locally asymptotically stable on the sliding domain  $\Sigma_s$ . The disease-free equilibrium  $E_0^r$  is unstable, and the endemic equilibria  $E_{12}^v$  and  $E_{22}^v$  are virtual. Thus the pseudo-equilibrium  $E_s$  is globally asymptotically stable due to the nonexistence of all limit cycles, as shown in Fig. 12(b). If  $I_c > I_{12}$ , the disease-free equilibrium  $E_0^r$  and the endemic equilibrium

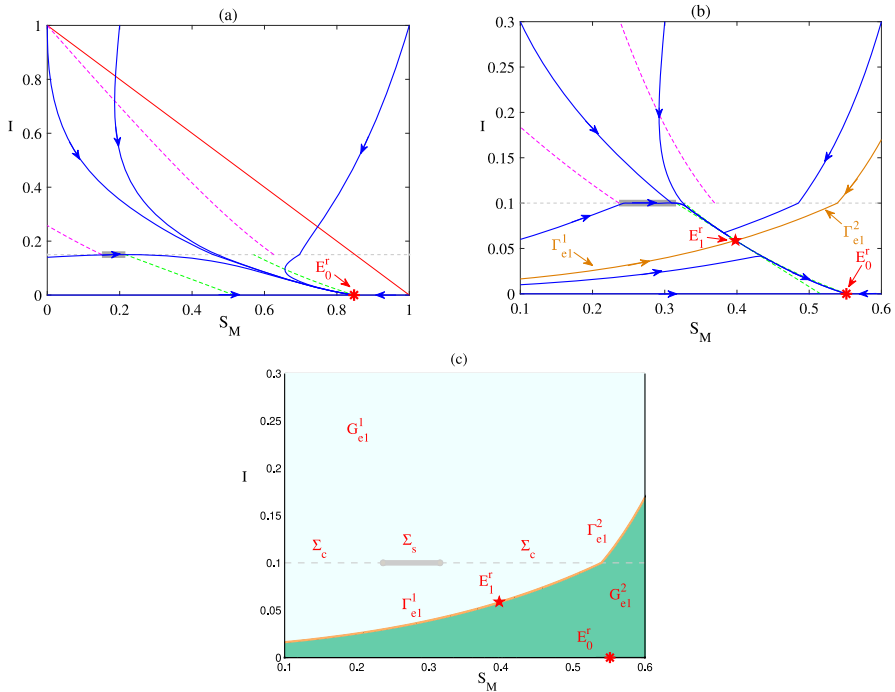


**Fig. 13** Phase plane of Filippov epidemic model (4). The parameter values are  $\beta = 0.415$ ,  $\mu = 0.01$ ,  $\gamma = 0.3$ ,  $d = 0.008$ ,  $\theta = 0.5$  and  $k = 5$ , with (a)  $\lambda = 0.1$ ,  $I_c = 0.15$ , (b)  $\lambda = 0.022134$ ,  $I_c = 0.1$ . (c) The basion of attraction for the two attractors  $E_1^r$  and  $E_0^r$ . The areas  $G_{el}^1$  and  $G_{el}^2$  are the basins of attraction for  $E_1^r$  and  $E_0^r$ , respectively. The orange curves  $\Gamma_{el}^1$ ,  $\Gamma_{el}^2$  represent the stable manifolds of  $E_1^r$ , and the red stars represent the saddle node point  $E_1^r$ . The red asterisks represent the real disease-free equilibrium  $E_0^r$

$E_{12}^r$  are real, while the endemic equilibrium  $E_{22}^v$  is virtual. We similarly derive that the endemic equilibrium  $E_{12}^r$  is globally asymptotically stable, as shown in Fig. 12(c).

If  $\mathcal{R}_0 < 1$ , there are six possible endemic equilibria,  $E_{11}$ ,  $E_{12}$ ,  $E_1$ ,  $E_{21}$ ,  $E_{22}$  and  $E_2$ , and one disease-free equilibrium,  $E_0$ , for system (4). The existence of endemic equilibria depends on the relationship of the threshold value  $R_{cj}$  ( $j = 1, 2$ ) and 1. Since  $R_{c1} > R_{c2}$ , we consider five cases in the following.

Case (C<sub>1</sub>):  $R_{c1} < 1$ .

There is only one disease-free equilibrium  $E_0$  and no endemic equilibrium for the system (4) in this scenario. There is no admissible pseudo-equilibrium for system (4). Hence the disease-free equilibrium  $E_0$  is globally asymptotically stable for system (4), as shown in Fig. 13(a).

Thus, the following conclusion can be obtained.

**Theorem 7** *The disease-free equilibrium  $E_0$  is globally asymptotically stable for the system (4) when  $R_{c1} < 1$ .*

Case (C<sub>2</sub>):  $R_{c1} = 1$ .

In this case, there exist a disease-free equilibrium  $E_0$  and an endemic equilibrium  $E_1$ . No pseudo-equilibrium exists for system (4). Note that  $E_1$  is a non-hyperbolic

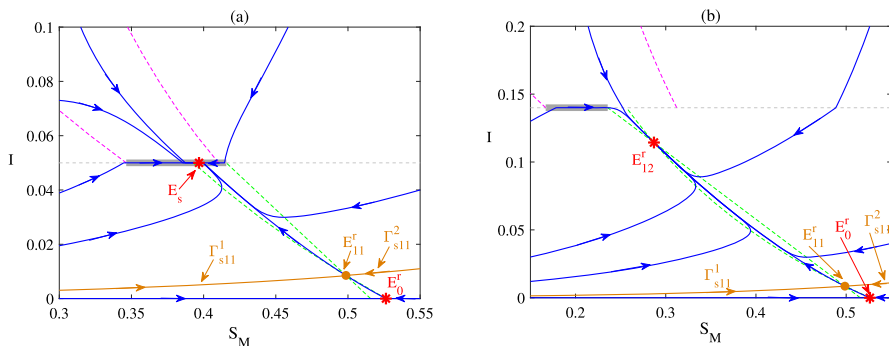


**Fig. 14** Phase plane of Filippov epidemic model (4).  $\beta = 0.415$ ,  $\mu = 0.01$ ,  $\lambda = 0.02$ ,  $\gamma = 0.3$ ,  $d = 0.008$ ,  $\theta = 0.5$  and  $k = 5$ , with (a)  $I_c = 0.05$ ; (b)  $I_c = 0.14$ . The orange circles represent the saddle points  $E_{11}^r$ , and the red asterisks represent the real endemic equilibrium  $E_{12}^r$ , the real disease-free equilibrium  $E_0^r$  and the pseudo-equilibrium  $E_s$ . The orange curves represent the stable manifolds of the saddle point  $E_{11}^r$ .

saddle node. Denote the two stable manifolds of the non-hyperbolic saddle node  $E_1$  as  $\Gamma_{e1}^1$  and  $\Gamma_{e1}^2$ , as shown in Fig. 13(b). Then  $\Gamma_{e1}^1$  and  $\Gamma_{e1}^2$  split the  $R_+^2$  plane into two subregions. Denote the set of all the points above (resp. below) the manifolds  $\Gamma_{e1}^1$  and  $\Gamma_{e1}^2$  as  $G_{e1}^1$  (resp.  $G_{e1}^2$ ), as shown in Fig. 13(c). We get the following result.

**Theorem 8** *The disease-free equilibrium  $E_0$  is globally asymptotically stable for system (4) when  $I_c < I_1$ . When  $I_c > I_1$ , coexistence of the two attractors  $E_1^r$  and  $E_0^r$  occurs for Filippov model (4). In particular, any orbit of system (4) initiating from  $Z_0 \in G_{e1}^1 \cup \Gamma_{e1}^1 \cup \Gamma_{e1}^2$  will approach  $E_1^r$ , while any orbit initiating from  $Z_0 \in G_{e1}^2$  will tend to  $E_0^r$ .*

**Proof** For any value of  $I_c$ , the disease-free equilibrium  $E_0^r$  is real. The endemic equilibrium  $E_1^v$  is virtual for  $I_c < I_1$ , and it is real, denoted by  $E_1^r$ , for  $I_c > I_1$ . If  $I_c < I_1$ , the disease-free equilibrium  $E_0^r$  is globally asymptotically stable for system (4), as shown in Fig. 13(a). If  $I_c > I_1$ , the endemic equilibrium  $E_1^r$  is real, and  $E_1^r$  is a non-hyperbolic saddle node. Let the initial point be  $Z_0 = (S_M^0, I^0)$ . Then any trajectory starting from  $Z_0 \in G_{e1}^1 \cup \Gamma_{e1}^1 \cup \Gamma_{e1}^2$  tends to the non-hyperbolic saddle node point  $E_1^r$ , while those trajectories initiating from  $Z_0 \in G_{e1}^2$  approach the disease-free equilibrium  $E_0^r$ , as shown in Fig. 13(b)–(c). Hence both the disease-free equilibrium  $E_0^r$  and the saddle node point  $E_1^r$  are the attractors of the system (4) when  $I_c > I_1$ .  $\square$

Case (C<sub>3</sub>):  $R_{c2} < 1 < R_{c1}$ .

In this case, the disease-free equilibrium  $E_0$  and two endemic equilibria  $E_{11}$ ,  $E_{12}$  exist for system (4) with  $S_{M11} > S_{M12}$  and  $I_{11} < I_{12}$ . According to Section 4, we know the pseudo-equilibrium  $E_s$  is admissible if and only if  $I_{11} < I_c < I_{12}$ . The endemic equilibrium  $E_{11}$  is a saddle. Denote the two stable manifolds of  $E_{11}$  as  $\Gamma_{s11}^1$  and  $\Gamma_{s11}^2$ . Then  $\Gamma_{s11}^1$  and  $\Gamma_{s11}^2$  split the  $R_+^2$  plane into two subregions,  $G_{s11}^1$  and  $G_{s11}^2$ , where the subregion  $G_{s11}^1$  (resp.,  $G_{s11}^2$ ) denotes the set of all points above (resp., below)  $\Gamma_{s11}^1$  and  $\Gamma_{s11}^2$ , as shown in Fig. 14(a).

We present the result in the following theorem and leave the proof to the appendix.

**Theorem 9** (i) If  $I_c < I_{11}$ , the disease-free equilibrium  $E_0^r$  is globally asymptotically stable for Filippov system (4).

(ii) If  $I_{11} < I_c < I_{12}$ , bistability of the equilibria  $E_s$  and  $E_0^r$  occurs for Filippov system (4). In particular, any orbit starting from  $Z_0 \in G_{s11}^1$  will approach the pseudo-equilibrium  $E_s$ , while any orbit starting from  $Z_0 \in G_{s11}^2$  will tend to the disease-free equilibrium  $E_0^r$ .

(iii) If  $I_c > I_{12}$ , bistability of the equilibria  $E_{12}^r$  and  $E_0^r$  occurs for Filippov system (4). In particular, any orbit starting from  $Z_0 \in G_{s11}^1$  will approach the endemic equilibrium  $E_{12}^r$ , while any orbit starting from  $Z_0 \in G_{s11}^2$  will tend to the disease-free equilibrium  $E_0^r$ .

Case (C<sub>4</sub>):  $R_{c2} = 1$ .

In this case, the disease-free equilibrium  $E_0$  and the endemic equilibria  $E_{11}$ ,  $E_{12}$  and  $E_2$  coexist for Filippov system (4) with  $S_{M11} > S_{M2} > S_{M12}$  and  $I_{11} < I_2 < I_{12}$ . The pseudo-equilibrium  $E_s$  is admissible for  $I_{11} < I_c < I_{12}$ . The equilibrium  $E_2$  is a non-hyperbolic saddle node. Denote the two stable manifolds of the saddle-node point  $E_2^r$  as  $\Gamma_{e2}^1$  and  $\Gamma_{e2}^2$ . If the equilibrium  $E_2^r$  is real but the equilibrium  $E_{11}^v$  is virtual, then  $\Gamma_{e2}^1$  and  $\Gamma_{e2}^2$  split the  $R_+^2$  plane into two subregions  $G_{e2}^1$  and  $G_{e2}^2$ , where  $G_{e2}^1$  (resp.,  $G_{e2}^2$ ) represents the set of all points above (resp., below)  $\Gamma_{e2}^1$  and  $\Gamma_{e2}^2$ , as shown in Fig. 15.

If both  $E_2^r$  and  $E_{11}^r$  are real, the two stable manifolds  $\Gamma_{s11}^1$  and  $\Gamma_{s11}^2$  of the saddle  $E_{11}^r$  and the other two stable manifolds  $\Gamma_{e2}^1$  and  $\Gamma_{e2}^2$  of the saddle node  $E_2^r$  split the  $R_+^2$  plane into three subregions:  $G_{e2}^1$ ,  $G_{s11}^2$  and  $G_s$ . Subregion  $G_{e2}^1$  is composed of all the points above  $\Gamma_{e2}^1$  and  $\Gamma_{e2}^2$ ; Subregion  $G_s$  is composed of all the points below  $\Gamma_{e2}^1$  and  $\Gamma_{e2}^2$  but above  $\Gamma_{s11}^1$  and  $\Gamma_{s11}^2$ ; and Subregion  $G_{s11}^2$  is composed of all the points below  $\Gamma_{s11}^1$  and  $\Gamma_{s11}^2$ , as shown in Fig. 15(c). We conclude the results in this scenario as following and leave the proof to the appendix.

**Theorem 10** (i) When  $I_c < I_{11}$ , coexistence of the attractors  $E_2^r$  and  $E_0^r$  occurs for Filippov system (4). In particular, any trajectory of system (4) initiating from  $Z_0 \in G_{e2}^1 \cup \Gamma_{e2}^1 \cup \Gamma_{e2}^2$  will approach the endemic equilibrium  $E_2^r$ , while any trajectory initiating from  $Z_0 \in G_{e2}^2$  will tend to the disease-free equilibrium  $E_0^r$ .

(ii) When  $I_{11} < I_c < I_2$ , coexistence of the three attractors  $E_2^r$ ,  $E_s$  and  $E_0$  occurs for Filippov system (4). In particular, any trajectory initiating from  $Z_0 \in G_{e2}^1 \cup \Gamma_{e2}^1 \cup \Gamma_{e2}^2$  will approach  $E_2^r$ , trajectories initiating from  $X_s \in G_s$  will approach  $E_s$ , and trajectories initiating from  $Z_0 \in G_{s11}^2$  will tend to  $E_0^r$ .

(iii) When  $I_2 < I_c < I_{12}$ , bistability of the equilibria  $E_s$  and  $E_0^r$  occurs for Filippov system (4). In particular, trajectories initiating from  $Z_0 \in G_{s11}^1$  will approach  $E_s$ , while those trajectories initiating from  $Z_0 \in G_{s11}^2$  will tend to  $E_0^r$ .

(iv) When  $I_c > I_{12}$ , bistability of equilibria  $E_{12}^r$  and  $E_0^r$  occurs for Filippov system (4). In particular, trajectories initiating from  $Z_0 \in G_{s11}^1$  will approach  $E_{12}^r$ , while those trajectories initiating from  $X_{02} \in G_{s11}^2$  will tend to  $E_0^r$ .

Case (C<sub>5</sub>):  $R_{c2} > 1$ .

In this scenario, the disease-free equilibrium  $E_0$  and four endemic equilibria  $E_{11}$ ,  $E_{12}$ ,  $E_{21}$  and  $E_{22}$  exist for the system (4) with  $S_{M11} > S_{M21} > S_{M22} > S_{M12}$  and

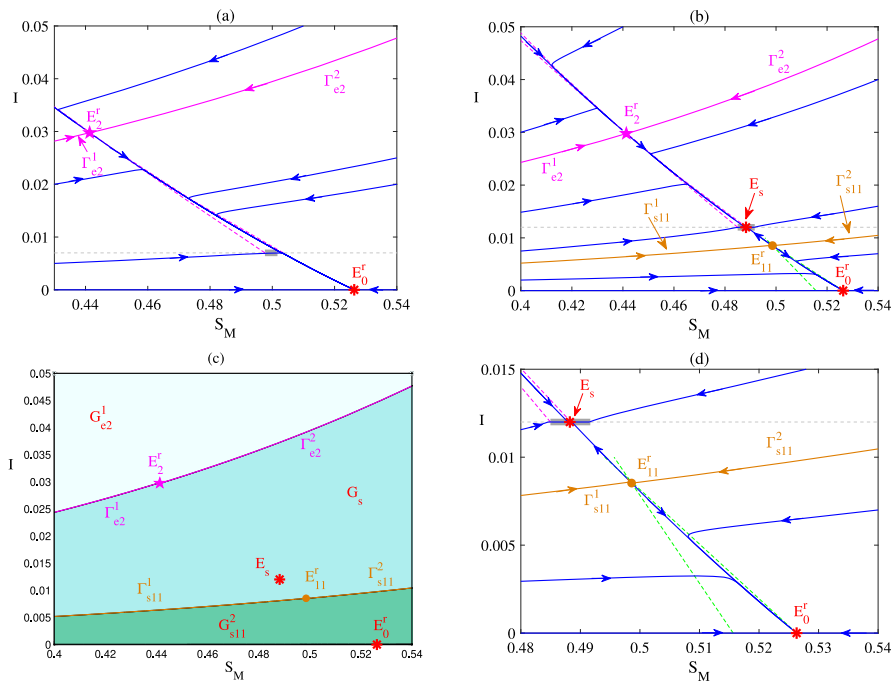


**Fig. 15** Phase plane of Filippov epidemic model (4). The parameter values are  $\beta = 0.415$ ,  $\mu = 0.01$ ,  $\lambda = 0.02$ ,  $\gamma = 0.3$ ,  $d = 0.008$ ,  $\theta = 0.5$  and  $k = 1.1663$ , with (a)  $I_c = 0.007$ ; (b)  $I_c = 0.012$ . The pink stars represent the saddle nodes  $E_2^r$ , the orange circles represent the saddle points  $E_{11}^r$ , and the red asterisks are the pseudo-equilibria  $E_s$  and the disease-free equilibria  $E_0^r$ . The pink (resp., orange) curves represent the stable manifolds of the saddle nodes  $E_2^r$  (resp., the saddle points  $E_{11}^r$ ). (c) The basins of attraction for the three attractors  $E_2^r$ ,  $E_s$  and  $E_0^r$ . The areas  $G_{e2}^1$ ,  $G_s$  and  $G_{s11}^2$  are the basins of attraction for  $E_2^r$ ,  $E_s$  and  $E_0^r$ , respectively. (d) Closeup of subplot (b)

$I_{11} < I_{21} < I_{22} < I_{12}$ . The pseudo-equilibrium  $E_s$  is admissible for  $I_{11} < I_c < I_{21}$  or  $I_{22} < I_c < I_{12}$ . Denote the two stable manifolds of the endemic equilibrium  $E_{21}$  as  $\Gamma_{s21}^1$  and  $\Gamma_{s21}^2$ . If the equilibrium  $E_{21}^r$  is real and the equilibrium  $E_{11}^v$  is virtual, then  $\Gamma_{s21}^1$  and  $\Gamma_{s21}^2$  split the  $R_+^2$  plane into two subregions:  $G_{s21}^1$  and  $G_{s21}^2$ . Subregion  $G_{s21}^1$  consists of all the points above the stable manifolds  $\Gamma_{s21}^1$  and  $\Gamma_{s21}^2$ , while Subregion  $G_{s21}^2$  consists of all the points below  $\Gamma_{s21}^1$  and  $\Gamma_{s21}^2$ .

If both  $E_{11}^r$  and  $E_{21}^r$  are real, the stable manifolds  $\Gamma_{s11}^1$  and  $\Gamma_{s11}^2$  of the saddle  $E_{11}^r$  and the stable manifolds  $\Gamma_{s21}^1$  and  $\Gamma_{s21}^2$  of the saddle  $E_{21}^r$  split the  $R_+^2$  plane into three subregions:  $G_{s21}^1$ ,  $G_e$  and  $G_{s11}^2$ . Subregion  $G_{s21}^1$  represents all the points above  $\Gamma_{s21}^1$  and  $\Gamma_{s21}^2$ ; Subregion  $G_e$  represents all the points below  $\Gamma_{s21}^1$  and  $\Gamma_{s21}^2$  but above  $\Gamma_{s11}^1$  and  $\Gamma_{s11}^2$ ; and Subregion  $G_{s11}^2$  represents all the points below  $\Gamma_{s11}^1$  and  $\Gamma_{s11}^2$ , as shown in Fig. 16. Thus we have the following result.

**Theorem 11** (i) When  $I_c < I_{11}$ , bistability of the equilibria  $E_{22}^r$  and  $E_0^r$  occurs for Filippov model (4). In particular, the trajectories of system (4) initiating from



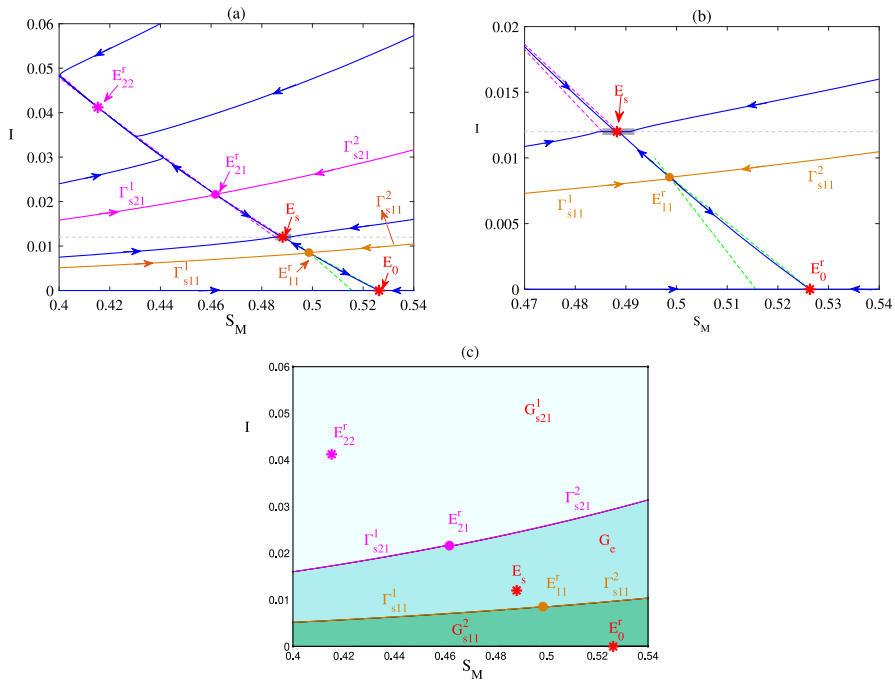


**Fig. 16** (a) Phase plane of Filippov epidemic model (4). The parameter values are  $\beta = 0.415$ ,  $\mu = 0.01$ ,  $\lambda = 0.02$ ,  $\gamma = 0.3$ ,  $d = 0.008$ ,  $\theta = 0.5$ ,  $k = 1.1$  and  $I_c = 0.012$ . The pink (resp., red) asterisks represent the real equilibria  $E_{22}^r$  (resp.,  $E_0^r$  and pseudo-equilibrium  $E_s$ ), the pink (resp., orange) circles represent the saddle points  $E_{21}^r$  (resp.,  $E_{11}^r$ ) and the pink (resp., orange) curves represent the stable manifolds of the saddle  $E_{21}^r$  (resp.,  $E_{11}^r$ ). (b) A closeup of subplot (a). (c) The basin of attraction for the three attractors  $E_{22}^r$ ,  $E_s$  and  $E_0^r$ . The areas  $G_{s21}^1$ ,  $G_e$  and  $G_{s11}^2$  are the basins of attraction for  $E_{22}^r$ ,  $E_s$  and  $E_0^r$ , respectively.

- $Z_0 \in G_{s21}^1$  will approach the endemic equilibrium  $E_{22}^r$ , while those trajectories initiating from  $Z_0 \in G_{s21}^2$  will tend to the disease-free equilibrium  $E_0^r$ .
- (ii) When  $I_{11} < I_c < I_{12}$ , multistability of the equilibria  $E_{22}^r$ ,  $E_s$  and  $E_0^r$  occurs for Filippov model (4). In particular, the trajectories of Filippov system (4) initiating from  $Z_0 \in G_{s21}^1$  will approach  $E_{22}^r$ , the trajectories initiating from  $Z_0 \in G_e$  will approach  $E_s$ , and those trajectories initiating from  $Z_0 \in G_{s11}^2$  will approach  $E_0^r$ .
- (iii) When  $I_{21} < I_c < I_{22}$ , bistability of the equilibria  $E_{22}^r$  and  $E_0^r$  occurs for Filippov model (4). In particular, any trajectory starting from  $Z_0 \in G_{s11}^1$  will tend to  $E_{22}^r$ , while those starting from  $Z_0 \in G_{s11}^2$  will tend to  $E_0^r$ .
- (iv) When  $I_{22} < I_c < I_{12}$ , bistability of the equilibria  $E_s$  and  $E_0^r$  occurs for Filippov system (4). In particular, any trajectory starting from  $Z_0 \in G_{s11}^1$  will ultimately go to  $E_s$ , while those starting from  $Z_0 \in G_{s11}^2$  will ultimately go to  $E_0^r$ .
- (v) When  $I_c > I_{12}$ , bistability of the equilibria  $E_{12}^r$  and  $E_0^r$  occurs for Filippov model (4). In particular, any trajectory starting from  $Z_0 \in G_{s11}^1$  will approach  $E_{12}^r$ , while those starting from  $Z_0 \in G_{s11}^2$  will tend to  $E_0^r$ .

The proof is found in the appendix.

For clarity, we summarize the above discussion and list all the possible regular equilibria, the existence of admissible pseudo-equilibrium, the attractors and the corresponding attraction regions of the targeted model (4) in different cases in the whole parameter space in Table 5.

In Table 5, the content in parentheses indicates whether the equilibrium is globally asymptotically stable or specifies its basin of attraction. For example,  $E_s(\text{GAS})$  indicates that the pseudo-equilibrium  $E_s$  is globally asymptotically stable in this scenario, and  $E_1^r(G_{e1}^1 \cup \Gamma_{e1}^1 \cup \Gamma_{e1}^2)$  indicates that the basin of attraction for the real equilibrium  $E_1^r$  consists of three parts,  $G_{e1}^1$ ,  $\Gamma_{e1}^1$  and  $\Gamma_{e1}^2$ , where  $\Gamma_{e1}^1$  and  $\Gamma_{e1}^2$  represent the two stable manifolds of  $E_1^r$  and  $G_{e1}^1$  is the subregion defined in Case ( $C_2$ ).

## 7 Discussion

We proposed a Filippov model with a threshold control strategy to explore the impact of social distancing on the spread and control of epidemic diseases. We divided the susceptible population into two compartments: fully susceptible individuals and social-distancing susceptibles. The threshold policy is defined as follows: once the proportion of infected individuals exceeds the threshold level  $I_c$ , social-distancing susceptibles intensify the measures of self-protection, reducing the infection rate to  $f(k, I)\theta\beta$ ; when the proportion of infected individuals falls below  $I_c$ , the infection rate of social-distancing susceptibles is  $\theta\beta$ . The proposed model exhibits rich and complex dynamic behaviours, including bistability and multistability of two or three equilibria.

Dynamic analysis of the free and control subsystems shows that there may be two, one or no endemic equilibria for the two subsystems with different parameter values, according to different threshold values  $R_{c1}$  and  $R_{c2}$ . We examined the critical conditions for the existence of admissible pseudo-equilibria as well as the sliding mode regions. By investigating the discontinuity-induced bifurcations, we found that either a boundary node (focus) bifurcation or a boundary saddle-node bifurcation occurs for the targeted model. A regular saddle-node collides with a tangent point to create a pseudo-saddle-node, leading to a boundary saddle-node bifurcation. Notably, another boundary saddle-node bifurcation occurs for the Filippov system when the regular saddle collides with the pseudo-node, creating a pseudo-saddle-node. This reveals that the choice of threshold values would significantly affect the dynamic behaviour.

We are mainly concerned about the impact of social-distancing strategies — which are intensified once the epidemic becomes severe — on the transmission of infectious diseases. To this end, we deliberately explore the dynamic behaviour of the targeted model as the threshold value varies, whereupon the social-distancing measures are adjusted. We find that when the basic reproduction number  $\mathcal{R}_0 > 1$ , the targeted model may stabilize at one of the regular equilibria or at the pseudo-equilibrium, depending on the threshold value  $I_c$ . This indicates that the disease can be contained at a specified level for a proper threshold level, which is a satisfactory control result if eradicating the disease is proven to be impossible. When  $\mathcal{R}_0 < 1$ , a series of interesting dynamic behaviours occur for the Filippov model. One, two or three attractors coexist for the targeted model with different threshold values. The disease-free equilibrium

**Table 5** Attractors and attraction regions for Filippov system (4). The content in parentheses indicates whether the equilibrium is globally asymptotically stable (GAS) or specifies its basin of attraction

Parameter values	Ranges of threshold	Attractors with attraction regions
$\mathcal{R}_0 > 1$	$I_c < I_{22}$	$E_{22}^r$ (GAS)
	$I_{21} < I_c < I_{22}$	$E_s$ (GAS)
	$I_c > I_{12}$	$E_{12}^r$ (GAS)
$\mathcal{R}_0 < 1$	$R_{c1} < 1$	$E_0^r$ (GAS)
		$E_0^r$ (GAS)
	$R_{c1} = 1$	$E_0^r$ (GAS)
		$E_0^r$ (GAS)
	$R_{c2} < 1 < R_{c1}$	$E_0^r$ ( $G_e^2$ ), $E_1^r$ ( $G_e^1 \cup \Gamma_{e1}^1 \cup \Gamma_{e1}^2$ )
		$E_0^r$ (GAS)
		$E_0^r$ ( $G_{s11}^2$ ), $E_s$ ( $G_{s11}^1$ )
		$E_0^r$ ( $G_{s11}^2$ ), $E_{12}^r$ ( $G_{s11}^1$ )
	$R_{c2} = 1$	$E_0^r$ ( $G_e^2$ ), $E_2^r$ ( $G_e^1 \cup \Gamma_{e2}^1 \cup \Gamma_{e2}^2$ )
		$E_0^r$ ( $G_{s11}^2$ ), $E_2^r$ ( $G_{e2}^1 \cup \Gamma_{e2}^1 \cup \Gamma_{e2}^2$ ), $E_s$ ( $G_s$ )
$R_{c2} > 1$	$I_c < I_{12}$	$E_0^r$ ( $G_{s11}^2$ ), $E_s$ ( $G_{s11}^1$ )
		$E_0^r$ ( $G_{s11}^2$ ), $E_{12}^r$ ( $G_{s11}^1$ )
	$I_c > I_{12}$	$E_0^r$ ( $G_{s21}^2$ ), $E_{22}^r$ ( $G_{s21}^1$ )
		$E_0^r$ ( $G_{s11}^2$ ), $E_{22}^r$ ( $G_{s11}^1$ )
	$I_{11} < I_c < I_{12}$	$E_0^r$ ( $G_{s11}^2$ ), $E_{22}^r$ ( $G_{s21}^1$ ), $E_s$ ( $G_e$ )
		$E_0^r$ ( $G_{s11}^2$ ), $E_{22}^r$ ( $G_{s11}^1$ )
	$I_{21} < I_c < I_{22}$	$E_0^r$ ( $G_{s11}^2$ ), $E_{22}^r$ ( $G_{s11}^1$ )
		$E_0^r$ ( $G_{s11}^2$ ), $E_s$ ( $G_{s11}^1$ )
	$I_{22} < I_c < I_{12}$	$E_0^r$ ( $G_{s11}^2$ ), $E_{12}^r$ ( $G_{s11}^1$ )
		$E_0^r$ ( $G_{s11}^2$ ), $E_{12}^r$ ( $G_{s11}^1$ )

is globally asymptotically stable for a proper threshold value, suggesting that the disease can be eradicated. Bistability of the regular endemic equilibrium or the pseudo-equilibrium and the disease-free equilibrium also occurs for the Filippov system. The most interesting outcome is that multistability of the regular endemic equilibrium, the pseudo-equilibrium and the disease-free equilibrium can occur for the system. These findings indicate that the dynamic behaviour of the proposed system depends not only on threshold values but also on the initial conditions. For a proper threshold value, if the initial proportion of infected individuals is sufficiently small, the infection can be ruled out or controlled at a previously given threshold value; otherwise, it may stabilize at a relatively high level.

It is worth mentioning that the reinforcement factor of social distancing and the proportion of social-distancing susceptibles who return to fully susceptible can significantly affect the proportion of infected individuals and that of social-distancing susceptibles at equilibrium. This suggests that the intensity and the duration of social distancing by the susceptibles involved can have a significant impact on the final number of infections.

From the perspective of model construction, we classified susceptible individuals into two groups: those who practice social distancing and those who do not. In our Filippov model, social-distancing susceptibles enhance social distancing once the infection increases in severity. In contrast, existing studies focusing on the impact of social distancing on disease transmission have several limitations. Some adopted smooth systems that overlook variations in social distancing behaviour over time (Collinson et al. 2015; Gevertz et al. 2021); others adopted Filippov systems but do not distinguish between susceptible individuals based on whether they adopt social distancing (Xiao et al. 2012; Wang and Xiao 2014; Zhang et al. 2024; Wang et al. 2020; Deng et al. 2021). While a few studies do formulate Filippov models and differentiate between the two types of susceptibles, they do not incorporate the dynamic strengthening of social-distancing intensity in response to the increased severity of the epidemic (Xiao et al. 2015). Our model exhibits bistability or tristability, where two or even three equilibria can coexist as attractors. In contrast, the other studies typically identify one attractor (Xiao et al. 2012; Wang and Xiao 2014; Zhang et al. 2024; Wang et al. 2020; Deng et al. 2021) or focus primarily on model validation and sensitivity analysis (Collinson et al. 2015; Gevertz et al. 2021; Xiao et al. 2015). From the perspective of disease control, we have found the steady-state regimes — healthy, low epidemic and high epidemic — under which infected individuals approach zero, a relatively low level or a relatively high level. This multilevel control outcome contrasts with other modelling studies, in which the long-term dynamics typically result in only one of the following scenarios: disease eradication, convergence to a single endemic equilibrium or periodic oscillations. In summary, our main findings demonstrate that a proper threshold policy can assist in controlling and combating an emerging infectious disease.

Our work has some limitations, which should be acknowledged. We assume that the rate at which full susceptibles become social-distancing susceptibles is constant, but in reality it may depend on the proportion of infectives or awareness programs. We assume that all infected individuals return to the fully susceptible state upon recovery; however, for most infectious diseases, infected individuals transition to a recovered

compartment after recovery due to some level of acquired immunity. Incorporating these effects into our model would result in a higher-dimensional system, which we leave to future work.

## Appendix

Here we present the proof of Theorems 2 and 9–11.

**Proof of Theorem 2** We solve  $\mathcal{R}_0 = 1$  with respect to  $\beta$  and set its critical value to  $\beta = \beta^*$ , where

$$\beta^* = \frac{(\lambda + \mu + d)(d + \gamma)}{\theta\lambda + d + \mu}.$$

In this scenario, the right-hand side of the control subsystem is as follows:

$$\begin{aligned} f_{21} &= \lambda(1 - I) - (\lambda + \mu + d)S_M - \frac{\beta\theta S_M I}{1 + kI}, \\ f_{22} &= (\beta - \gamma - d)I - \beta\left(1 - \frac{\theta}{1 + kI}\right)S_M I - \beta I^2. \end{aligned}$$

The Jacobian matrix of the control subsystem is

$$J_2(S_M, I) = \begin{pmatrix} -(\lambda + \mu + d) - \frac{\beta\theta I}{1 + kI} & -\lambda - \frac{\beta\theta S_M}{(1 + kI)^2} \\ -\beta(1 - \frac{\theta}{1 + kI})I & (\beta - \gamma - d) - \beta\left(1 - \frac{\theta}{(1 + kI)^2}\right)S_M - 2\beta I \end{pmatrix}.$$

Evaluating it at  $(E_0, \beta^*)$  yields

$$J_2(E_0) \Big|_{\beta=\beta^*} = \begin{pmatrix} -(\lambda + \mu + d) & -\lambda - \frac{\theta\lambda(d + \gamma)}{\theta\lambda + \mu + d} \\ 0 & 0 \end{pmatrix}.$$

The eigenvalues of the above matrix are 0 and  $-(\lambda + \mu + d)$ . The left and right eigenvectors corresponding to the zero eigenvalue are

$$v^l = (v_1^l, v_2^l) = (0, 1) \text{ and } v^r = (v_1^r, v_2^r)^T = \left( -\frac{\lambda(\theta\lambda + \mu + d) + \theta\lambda(d + \gamma)}{(\theta\lambda + \mu + d)(\lambda + \mu + d)}, 1 \right)^T.$$

Computing the nonzero second-order partial derivatives of  $f_{21}$  and  $f_{22}$  at  $(E_0, \beta^*)$ , we obtain

$$\begin{aligned} \frac{\partial^2 f_{22}}{\partial S_M \partial I} &= \frac{\partial^2 f_{22}}{\partial I \partial S_M} = -\beta^*(1 - \theta), & \frac{\partial^2 f_{22}}{\partial I^2} &= -\beta^* \frac{2k\theta\lambda}{\lambda + \mu + d} - \beta^*, \\ \frac{\partial^2 f_{22}}{\partial I \partial \beta} &= \frac{\theta\lambda + \mu + d}{\lambda + \mu + d}. \end{aligned}$$

Let  $x_1 = S_m$ ,  $x_2 = I$ . According to Castillo-Chavez and Song (2004), the two bifurcation parameters  $\tilde{a}$  and  $\tilde{b}$  can be calculated as follows:

$$\begin{aligned}\tilde{a} &= \sum_{k,i,j=1}^2 v_k^l v_i^r v_j^r \frac{\partial^2 f_{2k}}{\partial x_i \partial x_j} (E_0, \beta^*) \\ &= (d + \gamma) \frac{2\lambda(1 - \theta)(\theta\lambda + \mu + d + \theta(d + \gamma)) - (2k\theta\lambda + \lambda + \mu + d)(\theta\lambda + \mu + d)}{(\theta\lambda + \mu + d)^2}, \\ \tilde{b} &= \sum_{k,i=1}^2 v_k^l v_i^r \frac{\partial^2 f_{2k}}{\partial x_i \partial \beta} (E_0, \beta^*) = \frac{\theta\lambda + \mu + d}{\lambda + \mu + d} > 0.\end{aligned}$$

If  $\tilde{a} < 0$ , then a forward bifurcation occurs for the control subsystem at  $\mathcal{R}_0 = 1$ ; otherwise, if  $\tilde{a} > 0$ , then a backward bifurcation occurs for the control subsystem at  $\mathcal{R}_0 = 1$ .  $\square$

In the following, we present the detailed proof of Theorem 9.

**Proof of Theorem 9** When  $I_c < I_{11}$ , the disease-free equilibrium  $E_0^r$  is always real, and the endemic equilibria  $E_{11}^v$  and  $E_{12}^v$  are virtual by the above discussion. Hence the disease-free equilibrium  $E_0^r$  is globally asymptotically stable for the system (4).

When  $I_{11} < I_c < I_{12}$ , the pseudo-equilibrium  $E_s$  is admissible for the system (4), and it is locally asymptotically stable on the sliding domain  $\Sigma_s$ . In this scenario, the disease-free equilibrium  $E_0^r$  and the endemic equilibrium  $E_{11}^r$  are real, and the endemic equilibrium  $E_{12}^v$  is virtual. The disease-free equilibrium state  $E_0^r$  is locally asymptotically stable; while the endemic equilibrium  $E_{11}$  is a saddle. Any trajectory starting from  $Z_0 \in G_{s11}^1$  tends to the pseudo-equilibrium  $E_s$ , and any trajectory starting from  $Z_0 \in G_{s11}^2$  tends to the disease-free equilibrium  $E_0^r$ , as shown in Fig 14(a). Hence both the disease-free equilibrium  $E_0^r$  and the pseudo-equilibrium  $E_s$  are the attractors of system (4) in this scenario.

When  $I_c > I_{12}$ , the disease-free equilibrium  $E_0^r$  and the endemic equilibria  $E_{11}^r$ ,  $E_{12}^r$  are real for system (2). The real equilibria  $E_0^r$  and  $E_{12}^r$  are locally asymptotically stable, while  $E_{11}^r$  is a saddle point. Any trajectory starting from  $Z_0 \in G_{s11}^1$  tends to the endemic equilibrium  $E_{12}^r$ , and any trajectory from  $Z_0 \in G_{s11}^2$  tends to the disease-free equilibrium  $E_0^r$ , as shown in Fig. 14(b). Thus both the disease-free equilibrium  $E_0^r$  and the endemic equilibrium  $E_{12}^r$  are the attractors of system (4).  $\square$

Next we prove Theorem 10.

**Proof of Theorem 10** When  $I_c < I_{11}$ , the disease-free equilibrium  $E_0^r$  and the endemic equilibrium  $E_2^r$  are real, and the endemic equilibria  $E_{11}^v$  and  $E_{12}^v$  are virtual. There is no admissible pseudo-equilibrium for Filippov system (4). Thus any trajectory starting from  $Z_0 \in G_{e2}^1 \cup \Gamma_{e2}^1 \cup \Gamma_{e2}^2$  tends to the saddle node  $E_2^r$ , while any trajectory initiating from  $Z_0 \in G_{e2}^2$  tends to the disease-free equilibrium  $E_0^r$ . Hence, the disease-free equilibrium  $E_0^r$  and the saddle node point  $E_2^r$  are attractors for system (4).

When  $I_{11} < I_c < I_{12}$ , the pseudo-equilibrium  $E_s$  is admissible for the system (4), and it is stable, as shown in Fig. 5(e). There are two further possibilities to consider. If  $I_{11} < I_c < I_2$ , the disease-free equilibrium  $E_0^r$  and the endemic equilibria  $E_{11}^r$  and  $E_2^r$

are real, while the endemic equilibrium  $E_{12}^v$  is virtual. The disease-free equilibrium  $E_0^r$  and the pseudo-equilibrium  $E_s$  are locally asymptotically stable, the endemic equilibrium  $E_{11}^r$  is a saddle, and  $E_2^r$  is a non-hyperbolic saddle node, as shown in Fig. 15(b). Thus any trajectory initiating from  $Z_0 \in G_{e2}^1 \cup \Gamma_{e2}^1 \cup \Gamma_{e2}^2$  tends to the saddle node point  $E_2^r$ , any trajectory initiating from  $Z_0 \in G_s$  tends to the pseudo-equilibrium  $E_s$ , and any trajectory initiating from  $Z_0 \in G_{s11}^2$  tends to the disease-free equilibrium  $E_0^r$ , as shown in Fig. 15(b),(d). Hence, the endemic equilibrium  $E_2^r$ , the pseudo-equilibrium  $E_s$  and the disease-free equilibrium  $E_0^r$  are the attractors of Filippov system (4) for  $I_{11} < I_c < I_2$ , as shown in Fig. 15(c).

If  $I_2 < I_c < I_{12}$ , the disease-free equilibrium  $E_0^r$  and the endemic equilibrium  $E_{11}^r$  are real, while the endemic equilibria  $E_{12}^v$  and  $E_2^v$  are virtual. Furthermore,  $E_0^r$  is locally asymptotically stable, and  $E_{11}^r$  is a saddle point. Thus any trajectory initiating from  $Z_0 \in G_{s11}^1$  tends to the pseudo-equilibrium  $E_s$ , and any trajectory initiating from  $Z_0 \in G_{s11}^2$  tends to the disease-free equilibrium  $E_0^r$ . Hence, the disease-free equilibrium  $E_0^r$  and the pseudo-equilibrium  $E_s$  are the attractors of system (4) for  $I_2 < I_c < I_{12}$ .

When  $I_c > I_{12}$ , the disease-free equilibrium  $E_0^r$  and the endemic equilibria  $E_{11}^r$ ,  $E_{12}^r$  are real, the endemic equilibrium  $E_2^v$  is virtual, and there is no pseudo-equilibrium for the Filippov system (4). The disease-free equilibrium  $E_0^r$  and endemic equilibrium  $E_{12}^r$  are locally asymptotically stable, while the endemic equilibrium  $E_{11}^r$  is a saddle point. Similarly, any trajectory initiating from  $Z_0 \in G_{s11}^1$  tends to the endemic equilibrium  $E_{12}^r$ , and trajectories initiating from  $Z_0 \in G_{s11}^2$  eventually tend to the disease-free equilibrium  $E_0^r$ . Hence, the disease-free equilibrium  $E_0^r$  and the endemic equilibrium  $E_{12}^r$  are the attractors for Filippov system (4).  $\square$

In the following, we prove Theorem 11.

**Proof of Theorem 11** When  $I_c < I_{11}$ , the disease-free equilibrium  $E_0^r$  and the endemic equilibria  $E_{21}^r$ ,  $E_{22}^r$  are real, the endemic equilibria  $E_{11}^v$ ,  $E_{12}^v$  are virtual, and there is no admissible pseudo-equilibrium for Filippov system (4). The real equilibria  $E_0^r$  and  $E_{22}^r$  are locally asymptotically stable, and the real equilibrium  $E_{21}^r$  is a saddle. Thus any trajectory initiating from  $Z_0 \in G_{s21}^1$  tends to the endemic equilibrium  $E_{22}^r$ , while those initiating from  $Z_0 \in G_{s21}^2$  tend to the disease-free equilibrium  $E_0^r$ . So bistability of the two equilibria  $E_{22}^r$  and  $E_0^r$  occurs for Filippov model (4). Hence, two attractors  $E_{22}^r$  and  $E_0^r$  coexist for Filippov model (4) in this scenario.

When  $I_{11} < I_c < I_{21}$ , the pseudo-equilibrium  $E_s$  is admissible for system (4), and it is stable. In this scenario, the disease-free equilibrium  $E_0$  and the endemic equilibria  $E_{11}^r$ ,  $E_{21}^r$  and  $E_{22}^r$  are real, and the endemic equilibrium  $E_{12}$  is virtual. The real equilibria  $E_0^r$  and  $E_{22}^r$  are locally asymptotically stable, while the real equilibrium  $E_{11}^r$  and  $E_{21}^r$  are saddle points. Thus any trajectory initiating from  $Z_0 \in G_{s21}^1$  tends to the endemic equilibrium  $E_{22}^r$ , any trajectory initiating from  $Z_0 \in G_e$  tends to the pseudo-equilibrium  $E_s$ , and those initiating from  $Z_0 \in G_{s11}^2$  approach the disease-free equilibrium  $E_0^r$ . It follows that multi-stability of three equilibria  $E_{21}^r$ ,  $E_s$  and  $E_0^r$  occurs for Filippov model (4). Hence, there exist three attractors,  $E_{21}^r$ ,  $E_s$  and  $E_0^r$ , for the Filippov model (4) in this scenario.

When  $I_{21} < I_c < I_{22}$ , the disease-free equilibrium  $E_0$  and the endemic equilibria  $E_{11}^r$ ,  $E_{22}^r$  are real, the endemic equilibria  $E_{12}^v$  and  $E_{21}^v$  are virtual for system (4),

and the pseudo-equilibrium is not admissible. The real equilibria  $E_0^r$  and  $E_{22}^r$  are locally asymptotically stable, and the real equilibrium  $E_{11}^r$  is a saddle. Similarly, the stable manifolds  $\Gamma_{s11}^1$  and  $\Gamma_{s11}^2$  split the  $R_+^2$  plane into two subregions,  $G_{s11}^1$  and  $G_{s11}^2$ . Trajectories starting from  $Z_0 \in G_{s11}^1$  tend to the endemic equilibrium  $E_{22}^r$  and trajectories starting from  $Z_0 \in G_{s11}^2$  eventually tend to the disease-free equilibrium  $E_0^r$ . Hence bistability of  $E_{22}^r$  and  $E_0^r$  occurs for the Filippov model (4), suggesting two attractors for model (4).

When  $I_{22} < I_c < I_{12}$ , the disease-free equilibrium  $E_0^r$  and the endemic equilibrium  $E_{11}^r$  are real, while the endemic equilibria  $E_{12}^v$ ,  $E_{21}^v$  and  $E_{22}^v$  are virtual. The pseudo-equilibrium  $E_s$  is admissible for model (4), and it is stable. The real equilibrium  $E_0^r$  is locally asymptotically stable, while the real equilibrium  $E_{11}^r$  is a saddle. We similarly obtain that trajectories initiating from  $Z_0 \in G_{s11}^1$  tend to the pseudo-equilibrium  $E_s$  and trajectories initiating from  $Z_0 \in G_{s11}^2$  eventually tend to the disease-free equilibrium  $E_0^r$ . Hence bistability of  $E_0^r$  and  $E_s$  occurs for Filippov model (4), indicating two attractors for model (4) in this scenario.

When  $I_c > I_{12}$ , the disease-free equilibrium  $E_0^r$  and the endemic equilibria  $E_{11}^r$ ,  $E_{12}^r$  are real, while the endemic equilibria  $E_{21}^v$  and  $E_{22}^v$  are virtual. There is no admissible pseudo-equilibrium for Filippov model (4). The real equilibria  $E_0^r$  and  $E_{12}^r$  are locally asymptotically stable, while the real equilibrium  $E_{11}^r$  is a saddle. Similarly, trajectories starting from  $Z_0 \in G_{s11}^1$  tend to the endemic equilibrium  $E_{12}^r$ , and those trajectories starting from  $Z_0 \in G_{s11}^2$  eventually tend to the disease-free equilibrium  $E_0^r$ . Hence two attractors, the disease-free equilibrium  $E_0^r$  and the endemic equilibrium  $E_{12}^r$ , coexist for Filippov model (4) in this scenario, demonstrating bistability.  $\square$

**Acknowledgements** The authors are grateful to Cassandra Wooldridge for technical discussions. AW was supported by the National Natural Science Foundation of China (NSFC, 12271431, 12371514), WZ was supported by the National Natural Science Foundation of China (NSFC, 12471472), SS? was supported by an NSERC Discovery Grant. For citation purposes, please note that the question mark in "Smith?" is part of her name.

**Data Availability** The manuscript contains no data.

## References

- Brewer NT, Chapman GB, Gibbons FX et al (2007) Meta-analysis of the relationship between risk perception and health behaviour: the example of vaccination. *Health Psychol* 26(2):136
- Castillo-Chavez C, Song B (2004) Dynamical models of tuberculosis and their applications. *Math Biosci Eng* 1(2):361–404
- Chen K, Pun CS, Wong HY (2023) Efficient social distancing during the covid-19 pandemic: integrating economic and public health considerations. *Eur J Oper Res* 304(1):84–98
- Chen Z, Tsui JLH, Gutierrez B et al (2024) COVID-19 pandemic interventions reshaped the global dispersal of seasonal influenza viruses. *Science* 386(6722):eadq3003
- Cherif A, Barley K, Hurtado M (2016) Homo-psychologicus: reactionary behavioural aspects of epidemics. *Epidemics* 14:45–53
- Chu DK, Akl EA, Duda S et al (2020) Physical distancing, face masks, and eye protection to prevent person-to-person transmission of SARS-CoV-2 and COVID-19: a systematic review and meta-analysis. *Lancet* 395(10242):1973–1987
- Colley DG, Bustinduy AL, Secor WE et al (2014) Human schistosomiasis. *The Lancet* 383(9936):2253–2264



- Collinson S, Khan K, Heffernan JM (2015) The effects of media reports on disease spread and important public health measurements. *PLoS ONE* 10(11):e0141423
- Dashtbali M, Mirzaie M (2021) A compartmental model that predicts the effect of social distancing and vaccination on controlling covid-19. *Sci Rep-UK* 11(1):8191
- Deng J, Tang S, Shu H (2021) Joint impacts of media, vaccination and treatment on an epidemic Filippov model with application to COVID-19. *J Theor Biol* 523:110698
- Di Guilmi C, Galanis G, Baskozos G (2022) A behavioural SIR model: implications for physical distancing decisions. *Rev Behav Econ* 9(1):45–63
- Diaby M (2015) Stability analysis of a schistosomiasis transmission model with control strategies. *Biomath* 4(1):1504161
- d'Onofrio A, Manfredi P (2022) Behavioral SIR models with incidence-based social-distancing. *Chaos Soliton Fract* 159:112072
- Dryhurst S, Schneider C R, Kerr J, et al. (2022) Risk perceptions of COVID-19 around the world. Routledge, 162–174
- Duan Y, Shang B, Liang W et al (2022) Predicting hand washing, mask wearing and social distancing behaviours among older adults during the covid-19 pandemic: an integrated social cognition model. *BMC Geriatr* 22(1):91
- Epstein JM, Parker J, Cummings D et al (2008) Coupled contagion dynamics of fear and disease: mathematical and computational explorations. *PLoS ONE* 3(12):e3955
- Gevertz JL, Greene JM, Sanchez-Tapia CH et al (2021) A novel covid-19 epidemiological model with explicit susceptible and asymptomatic isolation compartments reveals unexpected consequences of timing social distancing. *J Theor Biol* 510:110539
- Gollwitzer A, McLoughlin K, Martel C et al (2022) Linking self-reported social distancing to real-world behaviour during the COVID-19 pandemic. *Soc Psychol Pers Sci* 13(2):656–668
- Gong Y, Wang A, Guo J et al (2022) Modelling the impact of media-induced social distancing on the containment of COVID-19 in Beijing. *Discrete Dyn Nat Soc* 2022(1):3954598
- Huang H, Chen Y, Yan Z (2021) Impacts of social distancing on the spread of infectious diseases with asymptomatic infection: a mathematical model. *Appl Math Comput* 398:125983
- Jain K, Bhatnagar V, Prasad S et al (2022) Coupling fear and contagion for modeling epidemic dynamics. *IEEE T Netw Sci Eng* 10(1):20–34
- Koo JR, Cook AR, Park M et al (2020) Interventions to mitigate early spread of SARS-CoV-2 in Singapore: a modelling study. *Lancet Infect Dis* 20(6):678–688
- Kristiansen IS, Halvorsen PA, Gyrd-Hansen D (2007) Influenza pandemic: perception of risk and individual precautions in a general population. Cross sectional study *BMC Public Health* 7:1–7
- Li T, Xiao Y, Heffernan J (2024) Linking spontaneous behavioral changes to disease transmission dynamics: behavior change includes periodic oscillation. *B Math Biol* 86(6):73
- Lobinska G, Pauzner A, Traulsen A et al (2022) Evolution of resistance to COVID-19 vaccination with dynamic social distancing. *Nat Hum Behav* 6(2):193–206
- Maharaj S, Kleczkowski A (2012) Controlling epidemic spread by social distancing: do it well or not at all. *BMC Public Health* 12:1–16
- Matrajt L, Leung T (2020) Evaluating the effectiveness of social distancing interventions to delay or flatten the epidemic curve of coronavirus disease. *Emerg Infect Dis* 26(8):1740
- Misra AK, Sharma A, Shukla JB (2011) Modeling and analysis of effects of awareness programs by media on the spread of infectious diseases. *Math Comput Model* 53(5–6):1221–1228
- Mpeshe SC, Nyerere N (2021) Modeling the dynamics of coronavirus disease pandemic coupled with fear epidemics. *Comput Math Method M* 2021(1):6647425
- Saha S, Samanta G, Nieto JJ (2022) Impact of optimal vaccination and social distancing on covid-19 pandemic. *Math Comput Simulat* 200:285–314
- Samanta S, Rana S, Sharma A et al (2013) Effect of awareness programs by media on the epidemic outbreaks: a mathematical model. *Appl Mathe Comput* 219(12):6965–6977
- Stockmaier S, Stroeimey N, Shattuck E C, et al. (2021) Infectious diseases and social distancing in nature. *Science*, 371(6533): eabc8881
- Tang B, Zhou W, Wang X et al (2022) Controlling multiple COVID-19 epidemic waves: an insight from a multi-scale model linking the behaviour change dynamics to the disease transmission dynamics. *B Math Biol* 84(10):106
- Ventura PC, Aleta A, Rodrigues FA et al (2022) Modeling the effects of social distancing on the large-scale spreading of diseases. *Epidemics* 38:100544

- Wang A, Xiao Y (2014) A Filippov system describing media effects on the spread of infectious diseases. *Nonlinear Anal-Hybrid Systems* 11:84–97
- Wang J, Zhang S, Wang L (2022) Global dynamics of a Filippov SIQR model with delayed relay control. *SIAM J Appl Math* 82(6):1879–1902
- Wang A, Xiao Y, Smith? RJ. (2020) Dynamics of a non-smooth epidemic model with three thresholds. *Theor Biosci*, 139: 47–65
- Willmore TJ (1960) The definition of Lie derivative. *Proc Edinb Math Soc* 12(1):27–29
- World Health Organization (2021). COVID-19 physical distancing. Available from: <https://www.who.int/westernpacific/emergencies/covid-19/information/physical-distancing>
- Xiao Y, Xu X, Tang S (2012) Sliding mode control of outbreaks of emerging infectious diseases. *Bull Math Biol* 74:2403–2422
- Xiao Y, Tang S, Wu J (2015) Media impact switching surface during an infectious disease outbreak. *Sci Rep-UK* 5(1):7838
- Yan Y, Malik AA, Bayham J et al (2021) Measuring voluntary and policy-induced social distancing behaviour during the COVID-19 pandemic. *P Natl Acad Sci USA* 118(16):e2008814118
- Zhang J, Tan S, Peng C et al (2023) Heterogeneous changes in mobility in response to the SARS-CoV-2 Omicron BA. 2 outbreak in Shanghai. *P Natl Acad Sci USA* 120(42):e2306710120
- Zhang Y, Zu J, Sun X (2024) Global dynamics of an epidemic model with a two-threshold policy. *Appl Math Model* 130:514–535
- Zhang Z, Zhang J, Li L et al (2024) Quantifying the effectiveness of brucellosis control strategies in northern China using a mechanistic and data-driven model. *Chaos Soliton Fract* 185:115121
- Zheng W, Deng X, Peng C et al (2023) Risk factors associated with the spatiotemporal spread of the SARS-CoV-2 Omicron BA. 2 variant–Shanghai Municipality, China, 2022. *China CDC Weekly* 5(5):97

**Publisher's Note** Springer Nature remains neutral with regard to jurisdictional claims in published maps and institutional affiliations.

Springer Nature or its licensor (e.g. a society or other partner) holds exclusive rights to this article under a publishing agreement with the author(s) or other rightsholder(s); author self-archiving of the accepted manuscript version of this article is solely governed by the terms of such publishing agreement and applicable law.